Report
R-22-02
July 2022

Simulating the thermo-mechanical evolution in the inner section of the Äspö Prototype Repository rock mass

Billy Fälth

SVENSK KÄRNBRÄNSLEHANTERING AB

SWEDISH NUCLEAR FUEL
AND WASTE MANAGEMENT CO

Box 3091, SE-169 03 Solna
Phone +46 8 459 84 00
skb.se

SVENSK KÄRNBRÄNSLEHANTERING

ISSN 1402-3091
SKB R-22-02
ID 1972464
July 2022

Simulating the thermo-mechanical evolution in the inner section of the Äspö Prototype Repository rock mass

Billy Fälth, Clay Technology AB

Abstract

The objective of the work that is presented in this report was to simulate the mechanical and the thermo-mechanical evolution in the inner section of the Prototype Repository rock mass. The focus was on the tangential stresses in the walls of the deposition holes.

The work was carried out by means of numerical modelling. A 3DEC model including the Prototype tunnel and the deposition holes was used. The basic assumption was to model the rock mass as a linear elastic continuum. For this assumption four modelling cases were considered, with different mechanical properties, thermo-mechanical properties and initial stress fields. To examine the potential impact of fractures, three model cases including a network of joint planes were considered. 3DEC's analytic logic was used for the temperature calculations. Based on the results, the following conclusions could be made:

- A good agreement between calculated rock mass temperatures and corresponding measurements can be obtained by using 3DEC's analytic logic. However, the model overestimated the temperatures at some positions in the innermost part of the tunnel. The overestimation of the temperature increase reached about 20 % at some locations near deposition holes 1 and 2. The overestimation was attributed to water movements and associated heat convection in the experiment.
- The overestimation of temperatures implies that the thermal stresses around the deposition holes were overestimated, particularly around hole 1 and 2. Around hole 3 and 4, where the highest stresses were found, the agreement between calculated and measured temperatures was considered acceptable.
- Given elastic continuum conditions (i.e., not considering the effects of fractures), the highest deposition hole wall stresses were always found near the tunnel floor. Adopting base case assumptions (homogeneous rock mass with "intact rock"-stiffness), no stress above 110 MPa was found after excavation. The heating increased the stresses such that the spalling strength (121 MPa) was exceeded. The highest stresses were generated in hole 3 after some 4 200 days of heating with stresses exceeding the spalling strength down to about 0.5 m below the tunnel floor.
- Variations in rock mass properties and background stress field may lead to higher stresses. In the three model cases with alternative rock mass stiffness distribution, higher background stress anisotropy and higher thermal expansion coefficient, respectively, the stresses were increased relative to those of the base case by almost 10 MPa in certain locations. The volumes with stresses exceeding the spalling strength increased, particularly in the case with higher stress anisotropy. In that case the model indicated possible initiation of spalling down to about 5 m depth in hole 3 and 4.
- Shear movements on fractures intersecting a deposition hole may locally perturb the stresses in the hole wall quite considerably. However, for the zero-pore pressure assumption, which was considered the most relevant of the two cases tested here, the shear displacements and the associated stress-perturbed volumes were modest. Hence, it is uncertain if any effects of fracture intersections will be observed after dismantling of the experiment.

In addition to the overestimation of temperatures, there are other factors suggesting that the stresses simulated here may be overestimates rather than underestimates:

- In all model cases considered here, the higher "intact rock" Young's modulus value was assumed for the rock mass around the deposition holes. Earlier work shows that assuming a lower "rock mass" Young´s modulus value everywhere instead of the higher "intact rock" value would give lower thermal stresses. In addition, the way the rock mass stiffness distribution was modelled here, with higher stiffness around the deposition holes, tends to give increased excavation stresses.
- No account was taken for the possible reductions of tangential stresses caused by swelling pressure in the bentonite buffer.

Given the modelling results presented here, with some model cases generating stresses several megapascals above the spalling strength, the possibility that spalling may have been initiated during heating cannot be excluded. This would be the case particularly in hole 3 and 4, in which the highest stresses were simulated and where the agreement between calculated and measured temperatures was best. However, results from earlier studies indicate that the small support of the pellet filling along the deposition hole wall may be sufficient to suppress the initiation of spalling.

Sammanfattning

Syftet med det arbete som presenteras i denna rapport var att simulera den mekaniska och termo-mekaniska utvecklingen i bergmassan i den inre sektionen av Prototypförvaret. Fokus var på de tangentiella spänningarna i deponeringshålsväggarna.

Arbetet utfördes via numerisk modellering. En 3DEC-modell, vilken inkluderade Prototyptunneln samt deponeringshålen användes. Utgångsantagandet var att modellera bergmassan som ett lineärelastiskt kontinuum. För detta antagande testades fyra fall med olika mekaniska egenskaper, termo-mekaniska egenskaper och initialspänningsfält. För att undersöka möjlig inverkan av sprickor, undersöktes även tre fall där ett spricknätverk inkluderades i modellen. 3DECs analytiska logik användes för temperaturberäkningarna. Baserat på resultaten kunde följande slutsatser dras:

- En god överensstämmelse mellan beräknade temperaturer i bergmassan och motsvarande uppmätta temperaturer kan erhållas med användande av 3DECs analytiska logik. Modellen överskattade emellertid temperaturerna i några positioner i den innersta delen av tunneln. Överskattningen av temperaturökningen uppgick till ca 20 % i några punkter i närheten av deponeringshål 1 och 2. Överskattningen hänfördes till vattenrörelser och associerad värmekonvektion i experimentet.
- Överskattningen av temperaturerna indikerar att de termiska spänningarna runt deponeringshålen överskattades, särskilt runt hål 1 och 2. Runt hål 3 och 4, där de högsta spänningarna erhölls, ansågs överensstämmelsen mellan beräknade och uppmätta temperaturer vara acceptabel.
- För elastiska kontinuumsförhållanden (effekter av sprickor inte inkluderade) erhölls alltid de högsta spänningarna i deponeringshålsväggarna nära tunnelgolvet. Vid applicerande av grundantagandet (homogen bergmassa med ”intakt berg”-styvhet), översteg inga spänningar 110 MPa efter utgrävning. Uppvärmningen ökade spänningarna så att gränsen för sprött brott (121 MPa) överskreds. De högsta spänningarna erhölls i hål 3 efter ca 4 200 dagars uppvärmning, då gränsen för sprött brott överskreds ner till ca 0,5 m djup under tunnelgolvet.
- Variationer i bergmassans egenskaper samt i bakgrundsspänningsfältet kan ge högre spänningar. I tre modellvarianter med alternativ fördelning av bergstyvheten, med högre spänningsanisotropi och med högre termisk utvidgningskoefficient ökade spänningarna i förhållande till spänningarna i grundmodellen med uppemot 10 MPa i vissa positioner. Volymerna med spänningar överstigande gränsen för spröda brott ökade, särskilt i fallet med högre spänningsanisotropi. I det fallet indikerade modellen att spröda brott möjligen kan initieras ned till ungefär 5 m djup i hål 3 och 4.
- Skjuvrörelser på sprickor som korsar ett deponeringshål kan lokalt störa spänningarna i deponeringshålsväggen avsevärt. För fallet utan portryck, vilket ansågs vara det mest relevanta av de två fall som testades här, blev emellertid skjuvrörelserna och de angränsande spänningsstörda volymerna modesta. Det är således osäkert om några effekter av korsande sprickor kommer att kunna observeras vid brytandet av experimentet.

Utöver överskattningen av temperaturerna finns det andra faktorer, vilka indikerar att spänningarna som simulerades här är överskattningar snarare än underskattningar:

- I alla modeller antogs elasticitetsmodulen för ”intakt berg” i bergmassan runt deponeringshålen. En tidigare studie visar att om ett lägre värde på elasticitetsmodulen motsvarande ”bergmassan” antas för hela modellvolymen i stället för det högre ”intakt berg”-värdet, så erhålls lägre termospänningar. Det sätt på vilket bergstyvhetsfördelningen modellerades här, med högre styvhet runt deponeringshålen, tenderar dessutom att ge ökade utgrävningsspänningar.
- Den möjliga reduktionen av tangentialspänningarna på grund av svälltryck i bentonitbufferten inkluderades inte i modellerna.

Givet de modelleringsresultat som presenteras här, med spänningar flera megapascal över gränsen för spröda brott i några fall, kan möjligheten att spröda brott blivit initierade under uppvärmningen inte uteslutas. Detta förefaller troligast i hål 3 och 4 där de högsta spänningarna simulerades och där överensstämmelsen mellan beräknade och uppmätta temperaturer är som bäst. Resultat från tidigare studier indikerar emellertid att ett litet mothåll från bentonitpelletsfyllningen längs deponeringshålsväggen kan vara tillräckligt för att undertrycka initiering av spröda brott.

Contents

1 Introduction

1.1 Background

The Prototype Repository is a large-scale field experiment aimed at assessing the response of the rock mass and the engineered barriers in a KBS-3 repository for spent nuclear fuel to changes in thermal, hydraulic, and mechanical conditions. The experiment is conducted at 450 m depth in the end of the TBM tunnel at the Äspö Hard Rock Laboratory (Figure 1-1).

The Prototype Repository was installed during 2001–2003 (Pusch et al. 2004). The experiment comprises six vertical full-scale deposition holes drilled from the tunnel floor. There are two sections separated by a concrete plug. Four of the deposition holes are in the inner section while the remaining two holes are in the outer section. Copper canisters surrounded by bentonite buffer were installed in all holes. To simulate the heat generation of the spent fuel, the canisters were equipped with electrical heaters. The tunnel was backfilled with a mix of crushed rock and bentonite and was sealed in the outer end by a concrete plug. A schematic overview of the experiment is shown in Figure 1-2 and geometric data are presented in Table 1-1.

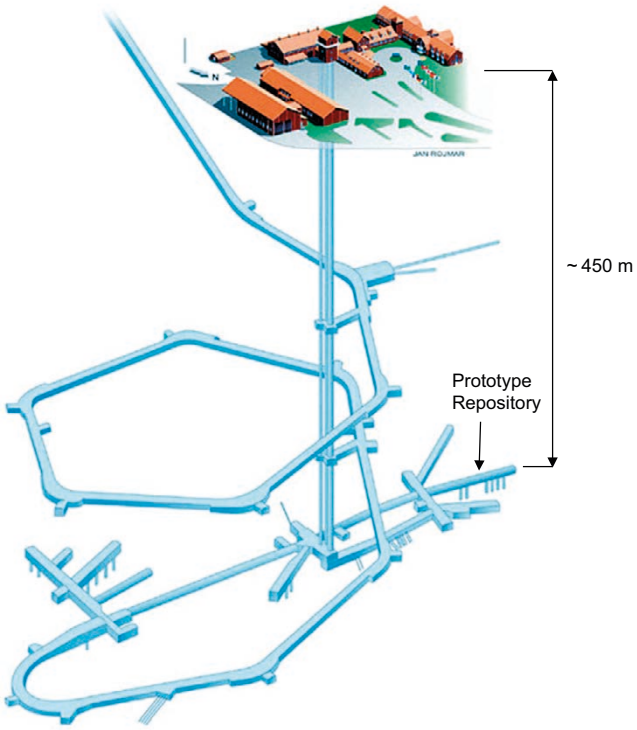

Figure 1-1. *Overview of the Äspö Hard Rock Laboratory and the location of the Prototype Repository (redrawn from Fransson et al. 2012).*

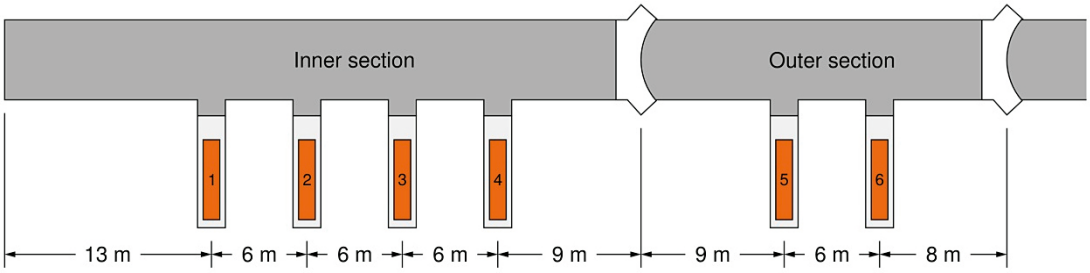

Figure 1-2. *Schematic overview of the Prototype Repository.*

Table 1-1. Geometric data of the Prototype Repository (after Kristensson and Hökmark 2007).

Deposition hole depth	~8 m	Bentonite thickness above the canister	1.5 m
Deposition hole diameter	1.75 m	Total tunnel length	63 m
Canister height	~5 m	Length of inner section	40 m
Canister diameter	1.05 m	Length of outer section	23 m
Bentonite thickness below the canister	0.5 m	Tunnel diameter	5 m

The outer section was dismantled during 2010 and 2011 (Svemar et al. 2016). The plan is that dismantling of the remaining inner section will start in the beginning of 2023. Prior to that, as a part of the planning of the dismantling work, predictive simulations of the thermo-mechanical response of the rock mass in the inner section have been carried out. The results from these simulations are described in this report.

1.2 Previous work

In conjunction with the dismantling of the outer section, numerical simulations were performed to estimate the thermo-mechanical evolution in the Prototype Repository rock mass. Using the finite element program Code_Bright (CIMNE 2004) and the 3-dimensional Distinct Element Code 3DEC (version 5.0) (Itasca 2013), Lönnqvist and Hökmark (2015) simulated the temperature evolution as well as the stress evolution in the rock, with particular focus on the stress evolution around the deposition holes in the outer section. Their model catalogue included linear elastic continuum models as well as models where fractures were explicitly modelled. Based on their simulation results, Lönnqvist and Hökmark made the following general conclusions:

- By applying 3DEC's analytical thermal logic, and hence assuming homogeneous and isotropic thermal properties in the models, a good agreement between simulated and measured temperatures in the outer section was obtained. In the inner section, however, the models tended to overpredict the temperatures. This could be attributed to water movements, and associated heat convection, out from the inner section.
- The locations with the highest stresses around the deposition holes as simulated by the models were generally in good agreement with the observed acoustic emissions. Since the location of the high-stress regions depends on the stress field, the orientation of the stress field in the Prototype Repository rock mass appeared to be well constrained by the stress models applied in the simulations.
- The potential for spalling in the deposition holes was assessed assuming the spalling strength to be 121 MPa. Given this, no systematic occurrence of spalling (other than locally close to the tunnel floor) was predicted by the models. The result agreed with the observations; no signs of any systematic stress-induced damage was observed in the deposition holes after dismantling. The simulated tangential stresses in the upper parts of the deposition holes were close to the spalling limit after excavation. From these observations Lönnqvist and Hökmark concluded that it is unlikely that the actual background stresses are much higher than the stresses applied as model input.
- The simulated fracture shear movements and the associated stress redistribution effects were significant only close to the opening peripheries. At some distance from the openings, all fractures were in high compression and had considerable stability margins.

The results from the work of Lönnqvist and Hökmark (2015) confirmed the validity of the stress models developed for the Prototype Repository rock mass. Furthermore, even though the agreement between calculated and measured temperatures was fair at some locations in the inner section, the results confirmed the efficiency of using the analytic thermal solution in 3DEC to simulate the thermal evolution in a KBS-3 repository.

1.3 Objectives and scope

The objective of the work that is presented in this report was to simulate the mechanical and the thermo-mechanical evolution in the inner section of the Prototype Repository rock mass. The focus was on the tangential stresses in the walls of the deposition holes.

The work was carried out by means of numerical modelling using an approach like that applied by Lönnqvist and Hökmark (2015). A 3DEC model including the Prototype tunnel and the deposition holes was used. The basic assumption was to model the rock mass as a linear elastic continuum, for which four cases with different mechanical properties, thermo-mechanical properties and initial stress fields were tested. To examine the potential impact of fractures, three model cases including a network of joint planes were considered. The mechanical and thermo-mechanical continuum properties as well as the properties assumed for the joints were the same as those applied by Lönnqvist and Hökmark (2015).

As noted above, Lönnqvist and Hökmark (2015) concluded that the use of 3DEC's analytic logic for temperature calculations means that the temperatures in the inner section tend to be overestimated. Overestimating the temperatures also means that the thermal stresses will tend to be overestimated. However, to develop a thermal model of the Prototype Repository that provides a thermal solution in better agreement with measurements than that of Lönnqvist and Hökmark (2015) would require that a calibration of non-homogeneous thermal properties is performed. It would also require a different, more computer demanding, numerical approach to be used. Given the time frame of the present study and given that an overestimation of stresses is "conservative" from a spalling assessment point of view, 3DEC's analytic logic was used also for the calculations presented here.

2 Model description

The simulations were carried out using 3DEC, version 7.145 (Itasca 2020). 3DEC is a program that is suitable for the present problem since the response of the continuum as well as of fractures is considered.

2.1 Geometry

The model comprises a cube with edge length 200 m. The tunnel was located centrally in the model volume (Figure 2-1). The dimensions of the system with tunnel and deposition holes were according to the specifications reported by Goudarzi (2021). The tunnel was circular with 5 m diameter and the deposition holes were 1.75 m in diameter and had a depth of 8.1 m (cf Table 1-1). Lönnqvist and Hökmark (2015) showed that the influence of the tunnel plug slots on the stress evolution in the deposition hole walls is negligible. Hence these were omitted in the model. The tunnel and the deposition holes in the inner section were created using a finer block structure than that in the outer section (Figure 2-1, right).

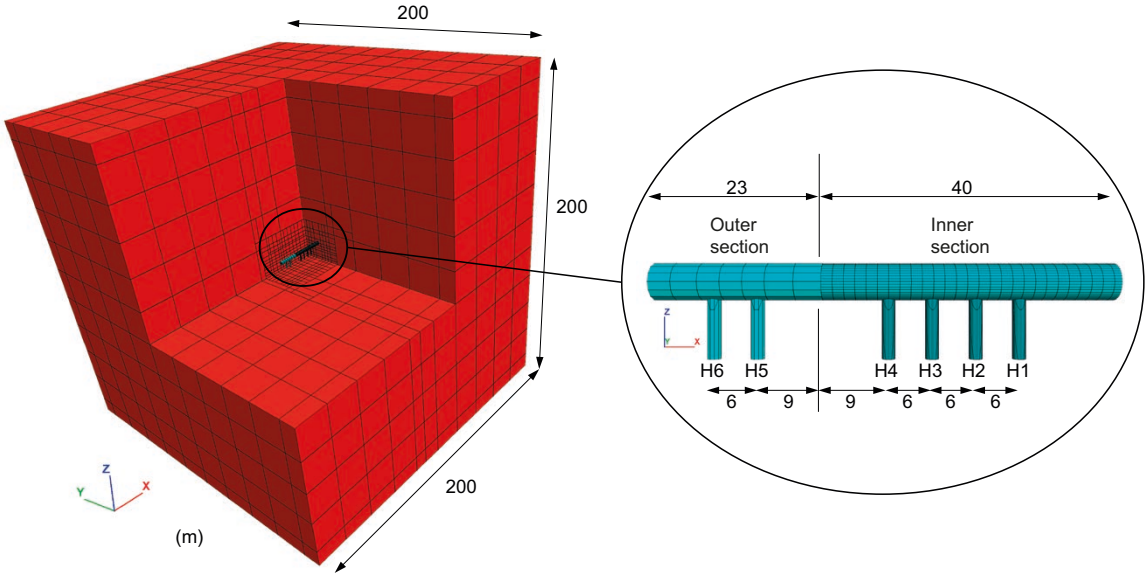

Figure 2-1. *The figure shows the block system of the model. The model comprises a cube with edge length 200 m where the Prototype Repository tunnel is located centrally in the model volume. Note that parts of the model are hidden in the figure.*

To examine the possible impact of fractures on the stresses in the deposition hole walls, seven joint planes were included in the inner section (Figure 2-2). The locations and orientations of the joint planes (Table 2-1) were based on visual inspection of Figure 6-3 to Figure 6-6 in Rhén and Forsmark (2001), which show the results of fracture mapping on the walls of the four deposition holes in the inner section. The intention here was to pick fractures such that a wide range of orientations was covered. There is no information regarding the sizes of the mapped fractures. All joint planes were cut through a model volume extending 40 m, 20 m and 22 m in the x-, y-, and z-directions, respectively. The tunnel axis goes approximately in the east–west direction (the trend of the tunnel is 266° in the RT 90 2.5 gon V :-15 system). Given the uncertainties in the orientations and locations of the fractures, it was schematically assumed that the tunnel trend is 270° (i.e., aligned with east–west) when the fracture joint planes were included in the model.

Table 2-1. Joint plane orientations (cf Figure 2-2).

Joint ID	Dip (deg)	Dip direction (deg)	From mapping of hole #
1046	30	125	1
1061	68	90	1
2069	80	285	2
3046	80	0	3
3075	44	297	3
4001	15	180	4
4019	58	10	4

Two model geometries were used. To evaluate the stresses in the deposition hole walls, an elastic continuum model was used (i.e., the effects of fractures not considered). When studying the potential impact of fractures, a model including the fracture joint planes (discontinuum) was analysed. For numerical efficiency, this model had a coarser discretisation as compared to the elastic continuum model.

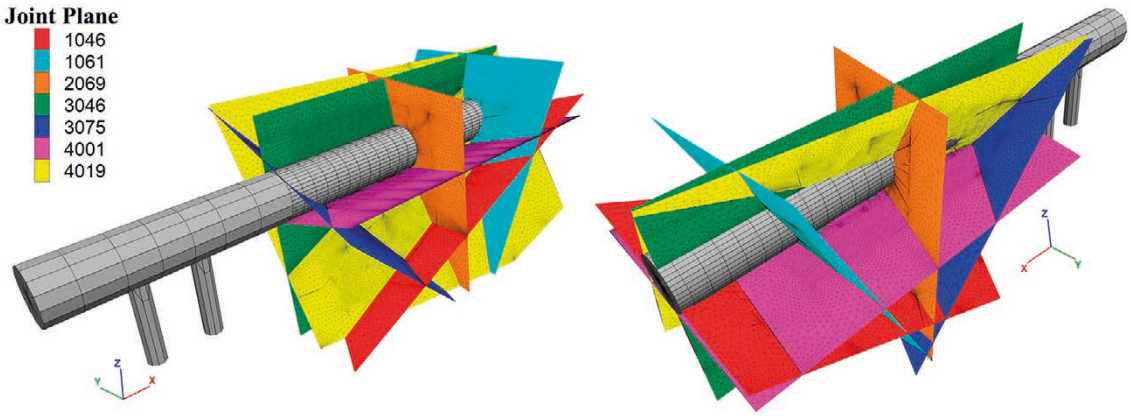

Figure 2-2. *Two views showing the tunnel and the seven joint planes included in the inner section.*

The model was discretised using tetrahedral finite difference elements. The discretisation was made finest around the deposition holes in the inner section (Figure 2-3) and then made gradually coarser toward the model boundaries. In the volumes surrounding the deposition holes in the inner section, the finite difference element edge length was set to be on average 5 cm in the elastic continuum model and 15 cm in the model including fractures (Figure 2-3). Note that the element sizes could deviate locally from these numbers depending on the block structure. The elastic continuum model contained about 11 million elements and the model with fractures had about 8.7 million elements.

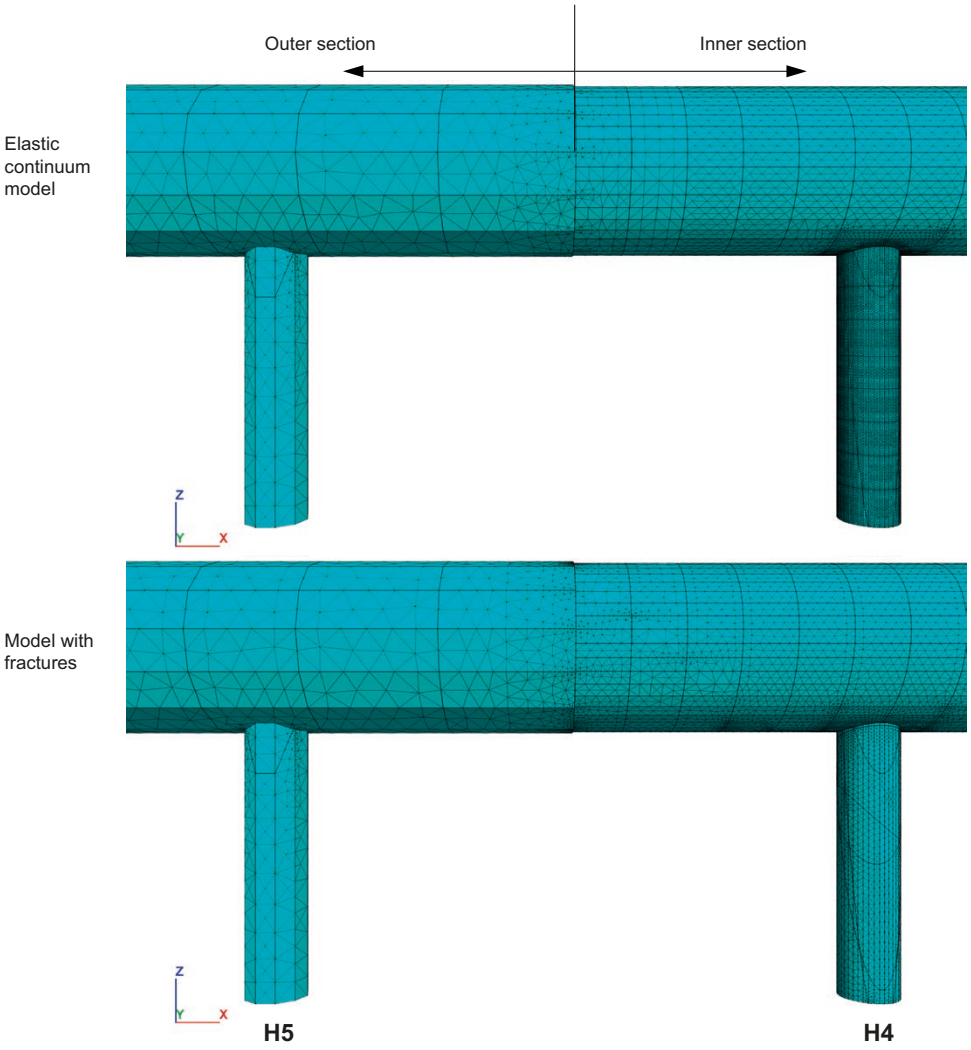

Figure 2-3. *Part of the tunnel showing the finite difference element mesh around the openings in the elastic continuum model (upper) and in the model with fractures (lower).*

2.2 Material properties

The rock between the fractures was modelled as a homogeneous, isotropic and linear elastic continuum. The fractures were assumed to respond to loads according to an idealised elasto-plastic material model with constant stiffnesses in both the normal and shear directions, and with failure according to a Coulomb criterion (Itasca 2020). The mechanical and thermo-mechanical property parameter values are listed in Table 2-2. These are the same as those applied by Lönnqvist and Hökmark (2015) when evaluating the stresses around the deposition holes in the outer section.

Table 2-2. Material property parameter values.

Component	Parameter	Unit	Value	Alternative
Rock mass	Thermal conductivity	W/(mK)	2.72	
	Thermal diffusivity	m^2/s	$1.275 \times 10e^{-6}$	
	Young's modulus, E	GPa	76 (intact rock)	55 (rock mass)
	Poisson's ratio, v	-	0.25	
	Density, ρ	kg/m^3	2 770	
	Coefficient of thermal expansion	K^{-1}	7×10^{-6}	8.3×10^{-6}
Fractures	Friction coefficient, μ	-	0.7*	
	Cohesion, c	MPa	0	
	Tensile strength	MPa	0	
	Normal stiffness, k_n	GPa/m	700	
	Shear stiffness, k_s	GPa/m	40	

* The value corresponds to a friction angle of 35°.

2.3 Boundary conditions

The horizontal stresses were not aligned with the model boundaries. To suppress unwanted displacements along the vertical boundaries, the nodes along these boundaries were locked in all directions. The horizontal boundaries were locked in the vertical direction (z-direction).

2.4 Initial conditions and heat loads

2.4.1 Background stress models and pore pressure

Two stress models were tested (Table 2-3). These are the same as those considered by Lönnqvist and Hökmark (2015) in their thermo-mechanical analysis of the outer section. The stress models are based on results from different stress measurements that have been carried out at the Äspö HRL. As noted in Section 1.2, the results by Lönnqvist and Hökmark (2015) indicated that the stress tensor orientation at the Prototype experiment site appears to be well in accord with the orientation in these stress models. Note that, for reference, the names of the stress models were the same here as those in the study by Lönnqvist and Hökmark (2015). The Case 1 model is the base case assumption. The Case 4 model was chosen as an alternative here since this is the model, out of those tested by Lönnqvist and Hökmark (2015), that tends to give the overall highest stresses around the deposition holes. The tensor orientation of the stress models relative to the Prototype Repository tunnel is illustrated in Figure 2-4. Note that the stress field was assumed to be homogeneous and no body forces due to gravity were considered.

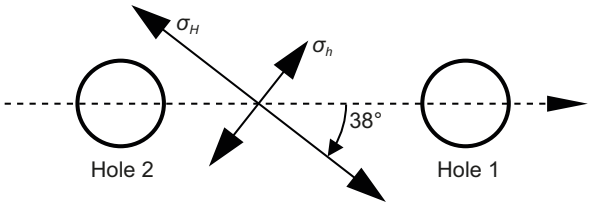

Figure 2-4. *Orientation of the horizontal stresses relative to the tunnel.*

Table 2-3. Stress models.

Model	σ_H		σ_h		σ_v	
	Magnitude (MPa)	Trend (°)	Magnitude (MPa)	Trend (°)	Magnitude (MPa)	Trend (°)
Case 1	28	304	14	214	12.8	-
Case 4	30	304	13	214	12.8	-

The effects of pore water pressure were considered in the cases with explicitly modelled fractures. The pore pressure was applied in the fracture network (not in the continuum) and was schematically assumed to be uniform, i.e., no account was taken for drainage into the openings and associated pressure gradients. The effects of variations in pore pressure were examined by making two end member assumptions:

1. Pore pressure is hydrostatic, corresponding to 450 m depth, i.e., 4.4 MPa, throughout the entire analysis.
2. Pore pressure is hydrostatic, corresponding to 450 m depth, i.e., 4.4 MPa, initially, but is set to zero during excavation of the openings and during the following heating phase.

2.4.2 Heat loads

The approach applied here for the thermo-mechanical calculation was the same as that used by Lönnqvist and Hökmark (2015). To model the thermal evolution in the rock mass, 3DEC's built-in analytic logic (Itasca 2020) was used. With this logic heat sources may be represented either by individual point sources, by grids of point sources or by line sources. The sources can be switched on at arbitrary times. Since linear thermal conduction is assumed, the temperature contributions from all heat sources can be superimposed to give the total temperature increase at each gridpoint in the model.

The power of a heat source can be either constant or exponentially decaying. To model the power evolution measured in the Prototype Repository experiment, heat sources with constant powers were switched on at appropriate time instances to obtain a stepwise heating power evolution (Figure 2-5).

Real canisters have a non-uniform heat flux distribution with higher surface flux at the top and bottom (e.g. Kristensson and Hökmark 2007). Hökmark and Fälth (2003) showed that a good representation of the heat flux distribution from a KBS-3V canister can be obtained by superposition of two line sources with uniform power distributions (Figure 2-6). This approach was used in SKB's safety analyses SR-Can and SR-Site (Hökmark et al. 2006, 2010) as well as in the thermo-mechanical simulations of the outer section of the Prototype Repository (Lönnqvist and Hökmark 2015). The approach was used here to model all six heaters in the experiment.

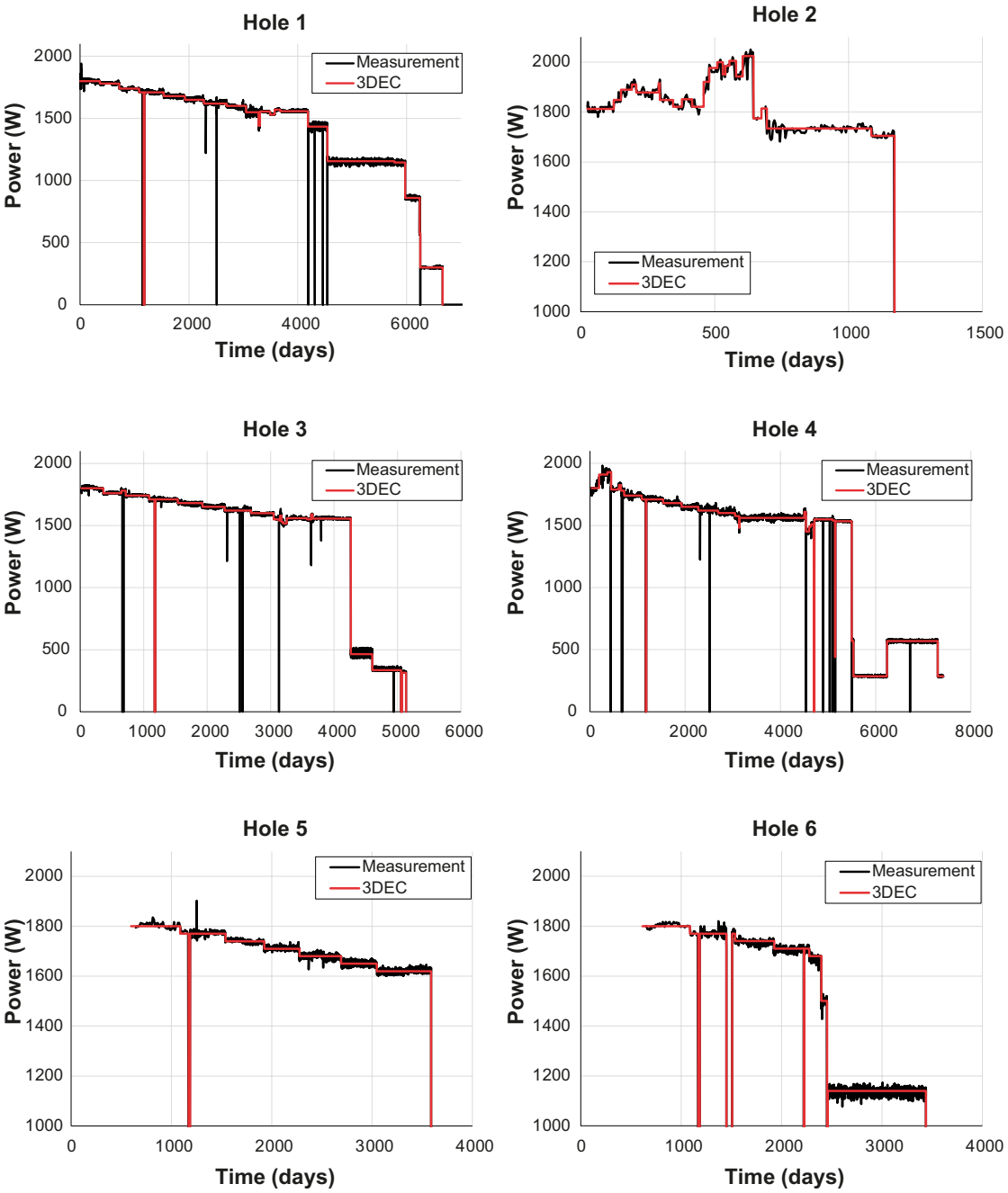

Figure 2-5. *Fit of the heat sources in the 3DEC model to the measured power evolutions in the Prototype Repository. Note that for hole 2, 5 and 6, values below 1 000 W mean that the power actually is zero.*

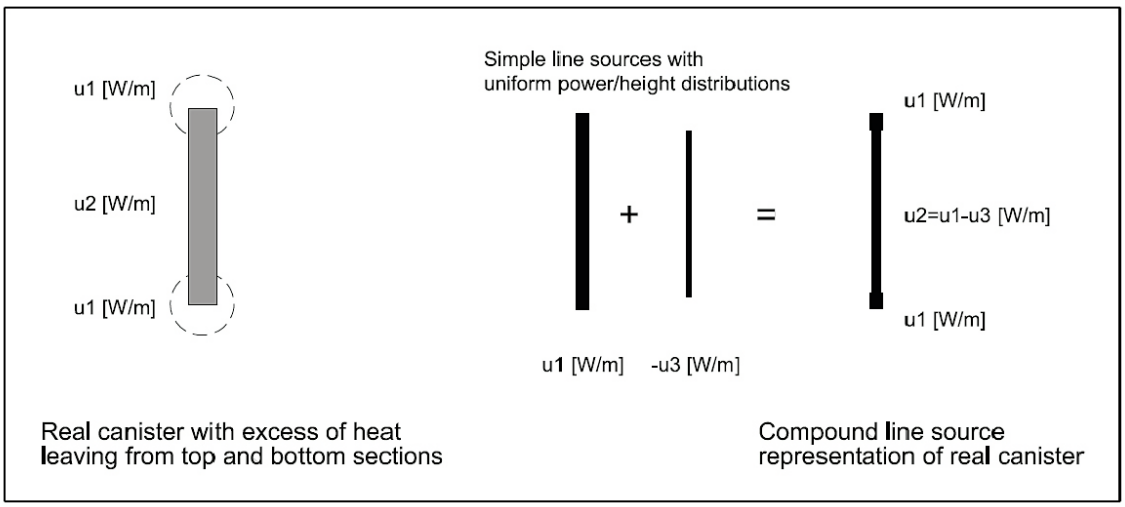

Figure 2-6. *Approach for creating compound line sources (from Hökmark and Fälth 2003).*

2.5 Calculation sequence

The calculation sequence included four main steps.

1. Initial equilibrium was established.
2. The tunnel was excavated.
3. The deposition holes were excavated.
4. Thermal loading was applied. This step included several substeps where the start and end of each substep coincided with the time instances at which the heating powers were changed (cf Figure 2-5).

Stresses and displacements could be evaluated after each main step/substep. The entire tunnel was excavated (calculation step 2) in one round. The same procedure was used for the deposition holes; all holes were excavated simultaneously. To avoid large, unbalanced forces and associated fracture displacement overshoots in the model containing fractures, fictitious high strength was assigned to the joints during excavation. The joint strength was then ramped down stepwise until the original strength was reached. After each strength reduction step, the model was cycled to equilibrium.

2.6 Simulated cases

A summary of the simulated cases is given in Table 2-4. The model denoted P1 is the base case. For reference, the model name (as well as stress model and properties) was the same as that in the study by Lönnqvist and Hökmark (2015). The effects of variations in the rock mass properties were examined in model P4. In this model, "intact rock" deformation modulus was assigned to the model volume surrounding the deposition holes while "rock mass" properties were assumed elsewhere (Figure 2-7). Model P4 here corresponds to model P4 in the Lönnqvist and Hökmark (2015) study. Then, there is one model (P1_Case4) where the alternative background stress model was applied and one model (P1_high_α) where the coefficient of thermal expansion was increased.

Three models with explicitly modelled fractures were analysed. In one of those models, the fracture joint planes were glued together (using the 3DEC join logic) to simulate an elastic and continuous rock mass. This model was used as reference when the effects of fractures were evaluated. The difference between the other two models with joint planes mechanically active regards the assumption of pore pressure (cf Section 2.4).

Table 2-4. Model map.

Model name	Description
Elastic continuum models	
P1	Base case. “Intact rock” properties everywhere (cf Table 2-2) and stress model Case 1
P4	Same as model P1 but with “intact rock” properties around deposition holes and “rock mass” properties elsewhere, see Figure 2-7
P1_Case4	Same as model P1 but with background stress model Case 4, cf Section 2.4
P1_high_α	Same as model P1 but with coefficient of thermal expansion increased to $\alpha = 8.3 \times 10^{-6}\ K^{-1}$
Models with fractures	
P1_fr	Properties and stress model as in model P1 but the effects of fractures are simulated. Zero pore pressure during excavation and heating
P1_fr_pp	Same as model P1_fr, but with full hydrostatic pore pressure throughout entire analysis
P1_fr_glued	Same as model P1_fr, but all joints are glued, i.e., an elastic and continuous rock mass is simulated.

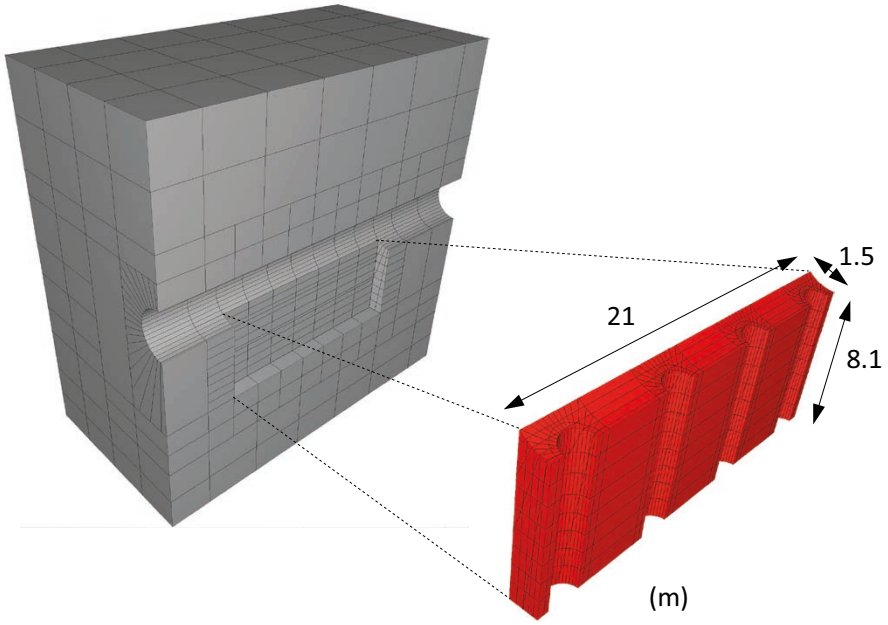

Figure 2-7. *In model P4, the volume surrounding the deposition holes was assigned “intact rock” Young’s modulus. The remaining of the model volume was assigned “rock mass” Young’s modulus.*

3 Results

The results presentation is divided into three sections. In the first section, the simulated temperature evolution is compared with the measurements made in the Prototype Repository rock mass. The stress evolution in the elastic continuum models is presented in the second section while the simulated effects of fractures on the stresses are presented in the third section. The focus is on the stress evolution in the walls of the deposition holes.

3.1 Temperature evolution

Simulated temperatures are plotted along with corresponding measurement data in Figure 3-1, Figure 3-2 and Figure 3-3. The temperature evolutions indicate that the heating power input was correctly applied. The agreement between calculation results and measurements is particularly good in the outer section. However, at some sensor positions in the inner section, the temperatures were overpredicted by the model after some 1 000–1 500 days. The overprediction tends to be more severe in the innermost part of the tunnel. Around hole 3 and 4 the agreement between calculated and measured temperatures can be considered acceptable.

As was noted by Lönnqvist and Hökmark (2015), the overprediction of temperatures can be attributed to changes in the drainage conditions that were initiated some 1 100 days after experiment start. This resulted in water movements and associated heat convection, which appears to give significant loss of heat. Such local effects cannot be modelled with the approach used here. The overprediction of temperatures means that the stresses around the deposition holes in the inner section, which was of main interest here, should be overpredicted rather than underpredicted by the model.

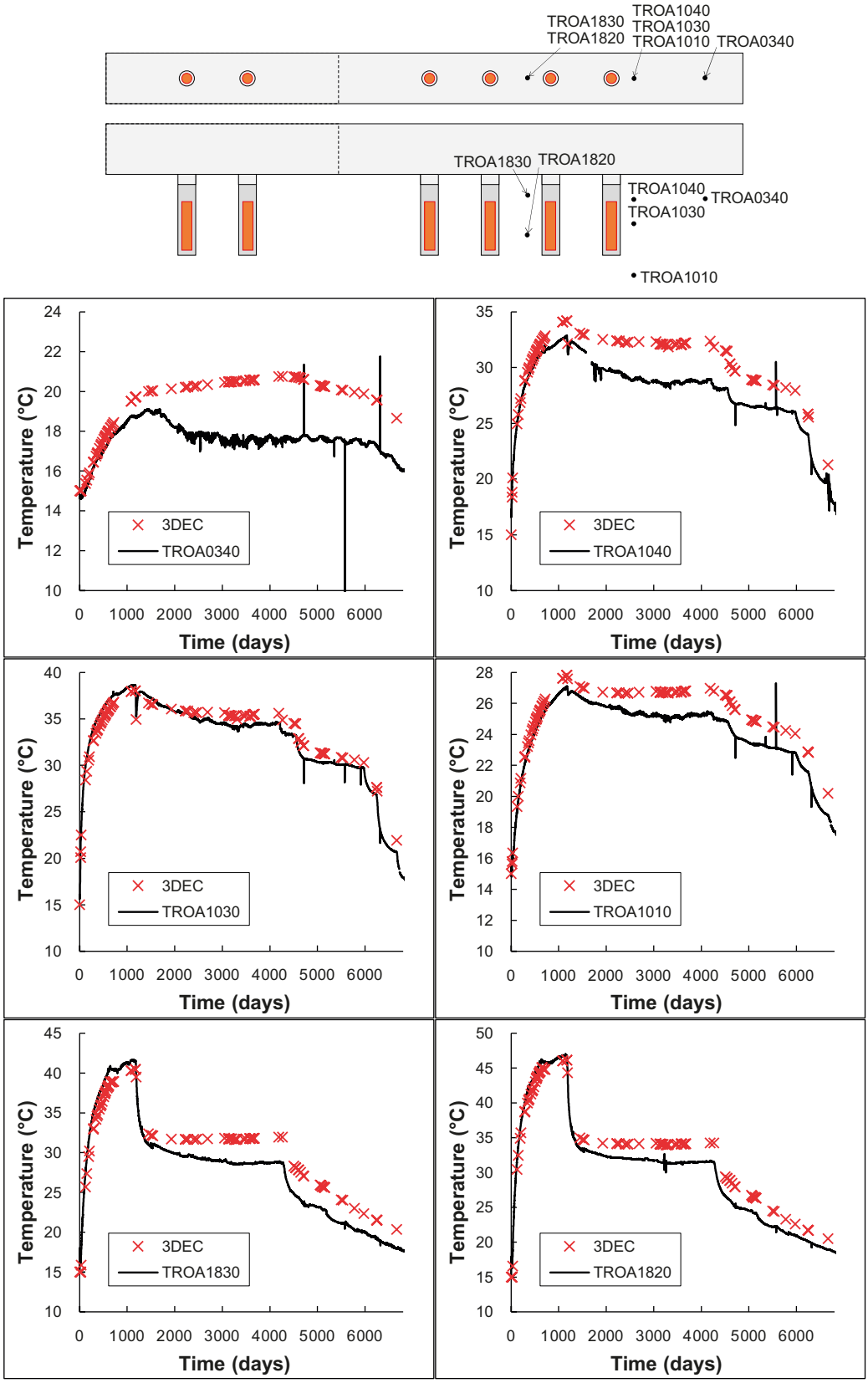

Figure 3-1. *Simulated temperature evolution plotted along with corresponding measurements.*

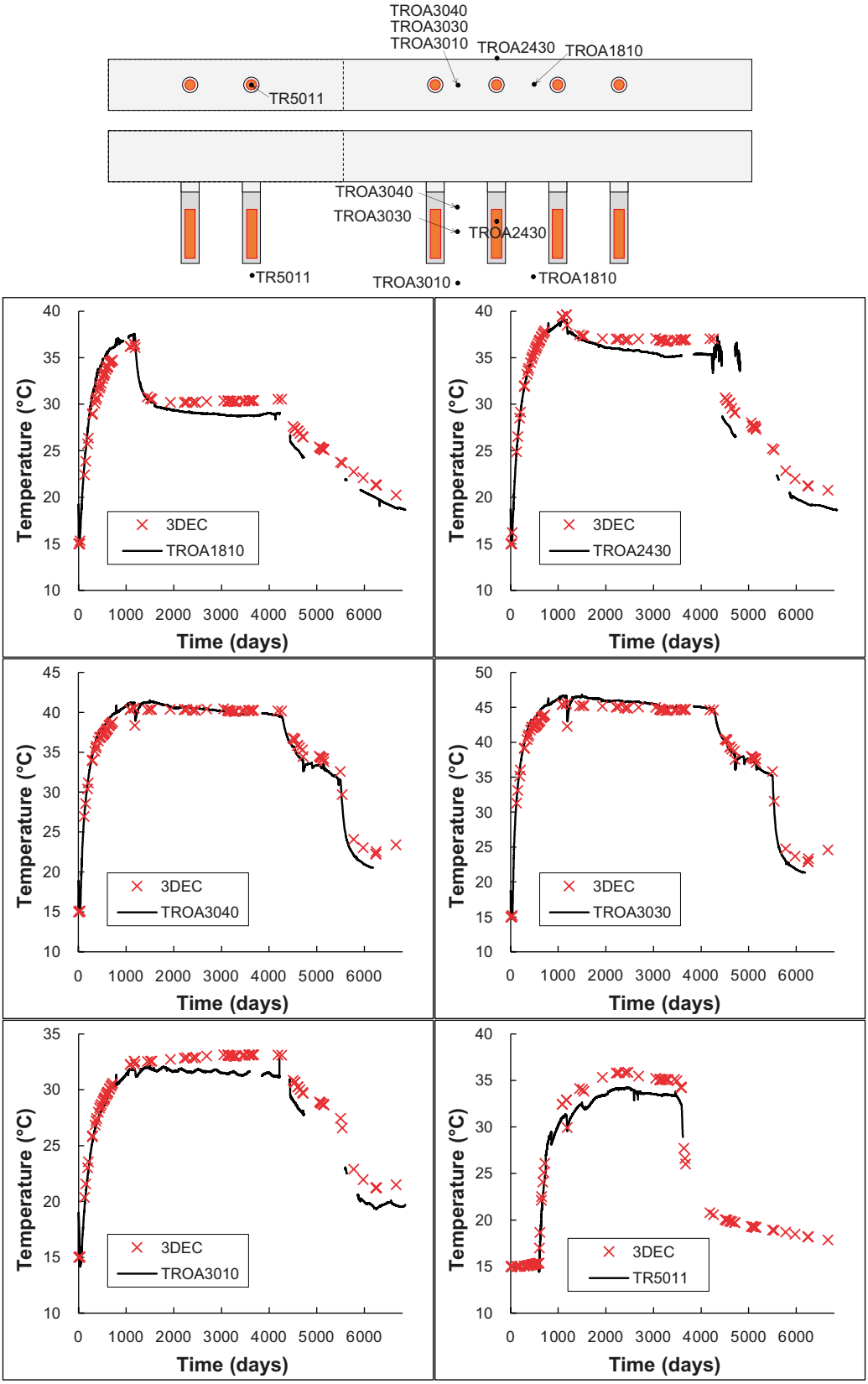

Figure 3-2. *Simulated temperature evolution plotted along with corresponding measurements.*

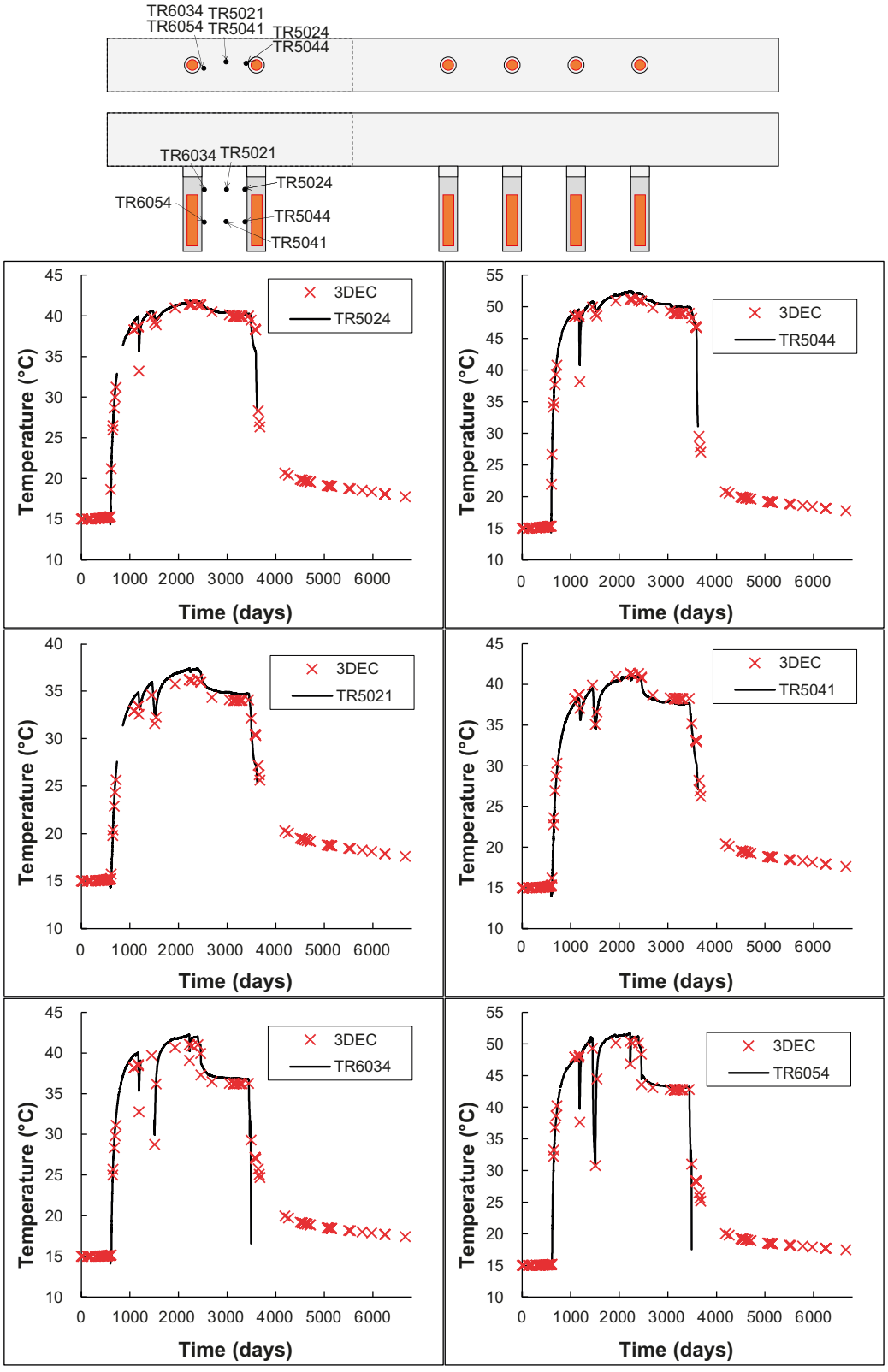

Figure 3-3. *Simulated temperature evolution plotted along with corresponding measurements.*

3.2 Stress evolution in the elastic continuum models

The focus in this study was on the stresses in the walls of deposition hole 1–4. It was of particular interest to examine the potential for the initiation of spalling. The potential for spalling was assessed assuming the spalling strength in unsupported holes to be 121 MPa, which corresponds to 57 % of the uniaxial compressive strength (Staub et al. 2004). In this section the stress evolution simulated by the elastic continuum models (i.e., no effects of fractures considered) is presented. It should be noted that comparing the stresses generated by an elastic continuum model with the spalling strength can give an indication of where and when there is risk for initiation of spalling. However, in the case the spalling limit is exceeded, other types of models are needed to obtain a more detailed prediction of the extent of the failure.

3.2.1 Base case model P1

The evolution of the major principal stress was monitored at two depths (0.5 and 5 m) below the tunnel floor in the most highly stressed region of the deposition hole walls. The stress evolution in the P1 model is shown in Figure 3-4. The locations of the monitoring points are indicated in the upper left panel in Figure 3-5. The following can be observed:

- The stresses after the two excavation stages are in good agreement with the stresses that were simulated at the corresponding positions by Lönnqvist and Hökmark (2015).
- Due to the stress concentrations around the tunnel, the stresses after completed excavation are highest at 0.5 m depth, closer to the tunnel floor.
- The start of heating means that the stresses at 5 m depth (at canister mid-height) increase to levels on par with those at 0.5 m depth. In the hottest region around canister mid-height, the stresses are sensitive to changes in the heating power and to the associated temperature changes in the rock. The temporary loss of power in all heaters (and the permanent shutdown of heater 2) after about 1 200 days (see Figure 2-5 and Figure 3-1 to Figure 3-3) is clearly reflected in the stress evolution, particularly at 5 m depth.
- The highest stresses are found around hole 3 and 4, where the temperatures are highest (see Section 3.1). At the monitoring point at 0.5 m depth the stresses almost reach the spalling limit.

Figure 3-5 shows contours of the major principal stress after excavation of the deposition holes and after 4 264 days of heating. The plots show (as also shown in Figure 3-4) that the highest stresses are found just below the tunnel floor. The stress increase induced by the heating means that the spalling strength may be exceeded in minor volumes close to the tunnel floor.

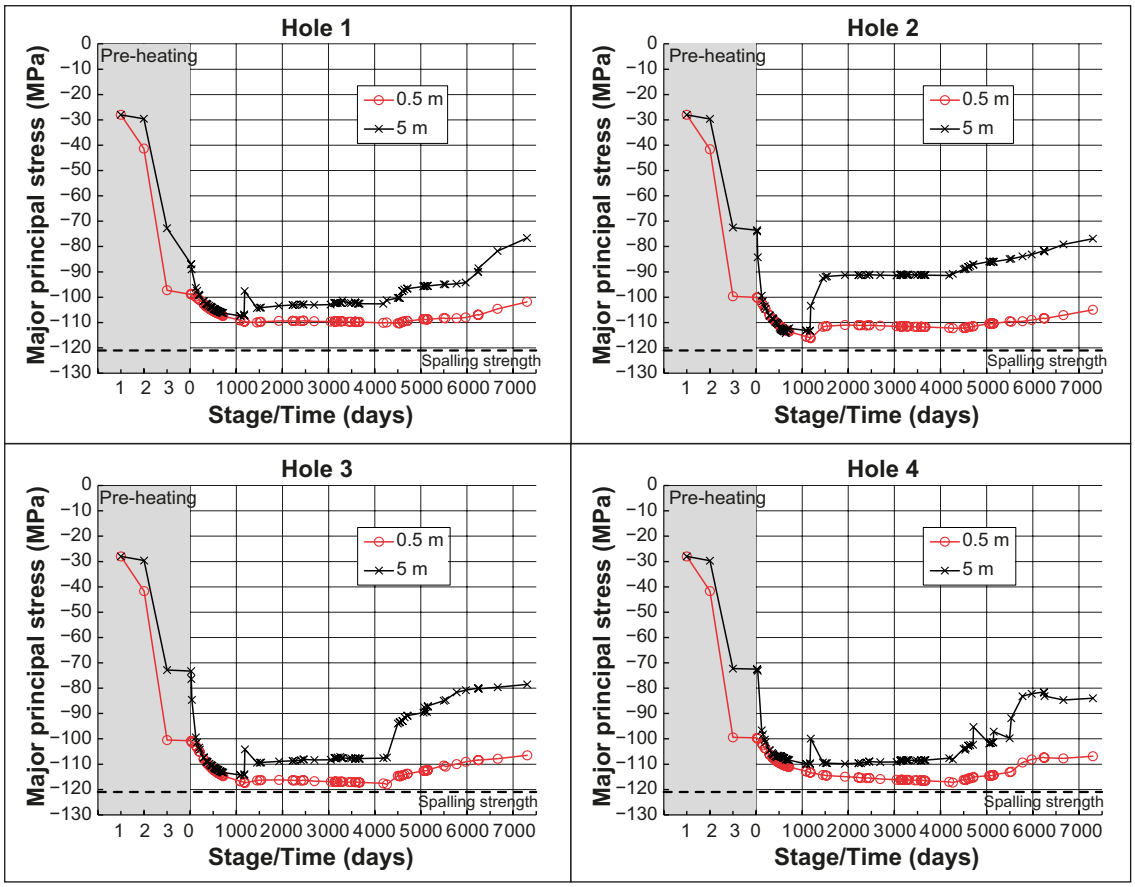

Figure 3-4. *Simulated evolution of major principal stress in the deposition hole walls in the P1 model. The results were monitored at two depths below tunnel floor, see Figure 3-5. The grey area represents the pre-heating stages: (1) initial equilibrium, (2) excavation of tunnel, and (3) excavation of deposition holes.*

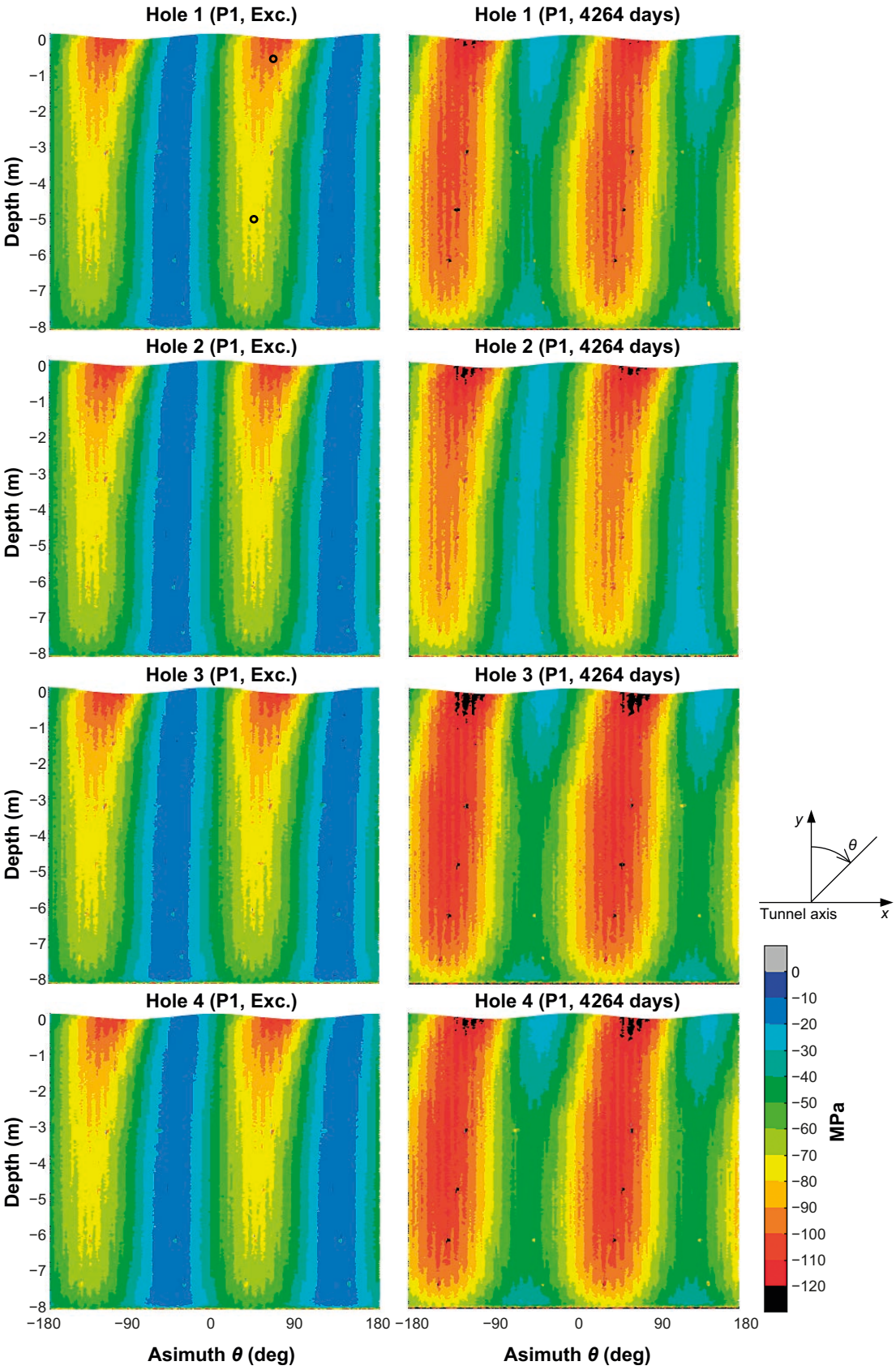

Figure 3-5. *Contours of major principal stress in the deposition hole walls in the P1 model after excavation and after 4 264 days of heating. The black circles in the upper left panel indicate locations for stress monitoring 0.5 m and 5 m below the tunnel floor.*

3.2.2 Impact of alternative stress model and material properties

The potential impact of variations in the background stress field and in the rock mass mechanical and thermo-mechanical properties was examined using the three alternative elastic continuum models. The simulated evolution of the major principal stress at two depths (0.5 and 5 m) below the tunnel floor is shown in Figure 3-6 while the stress distribution in the wall of deposition hole 3 for all elastic continuum models is shown in Figure 3-7. The stresses in Figure 3-7 correspond to the stages after excavation and after 4 264 days of heating, respectively (corresponding plots for all models and deposition holes are presented in Appendix A). The following can be observed:

- The alternative distribution of rock mass Young's modulus (model P4) (see Figure 2-7) has a more pronounced effect in the upper part of the deposition hole, close to the tunnel where the effects of the tunnel excavation and of the hole excavation are maximised. At 5 m depth the stresses generated in this model are on par with those generated in the P1 model.
- The larger background stress anisotropy in the P1_Case4 model leads to an increase of the stresses on the order of 10 MPa, both close to the tunnel and around canister mid-height. The effects are slightly more pronounced closer to the tunnel (Figure 3-6).
- The highest stresses were obtained close to the tunnel floor in hole 3 and 4 in the P4 and P1_Case4 models. At 0.5 m depth in these models, the stress exceeds the spalling limit during the time interval 1 000 – 4 500 days (approximately) of heating (Figure 3-6).
- The increase of the coefficient of thermal expansion (P1_high_α model) has more pronounced effects around canister mid-height where the temperature increase is highest. At 5 m depth in hole 3 and 4, this model case yields stresses that are on par with those of the P1_Case4 model during the heating phase (Figure 3-6).

All three alternative elastic continuum cases yield higher stresses during the heating phase as compared to the stresses generated in the base case P1 model. As in the P1 model, the stresses are highest in hole 3, where the spalling strength is exceeded by 5-6 MPa after 4 264 days of heating in the P1_Case4 model. For this model case, the contours in Figure 3-7 indicate possible initiation of spalling down to about 5 m depth in hole 3. A similar observation can be made also for hole 4 in Figure A-3 in Appendix A.

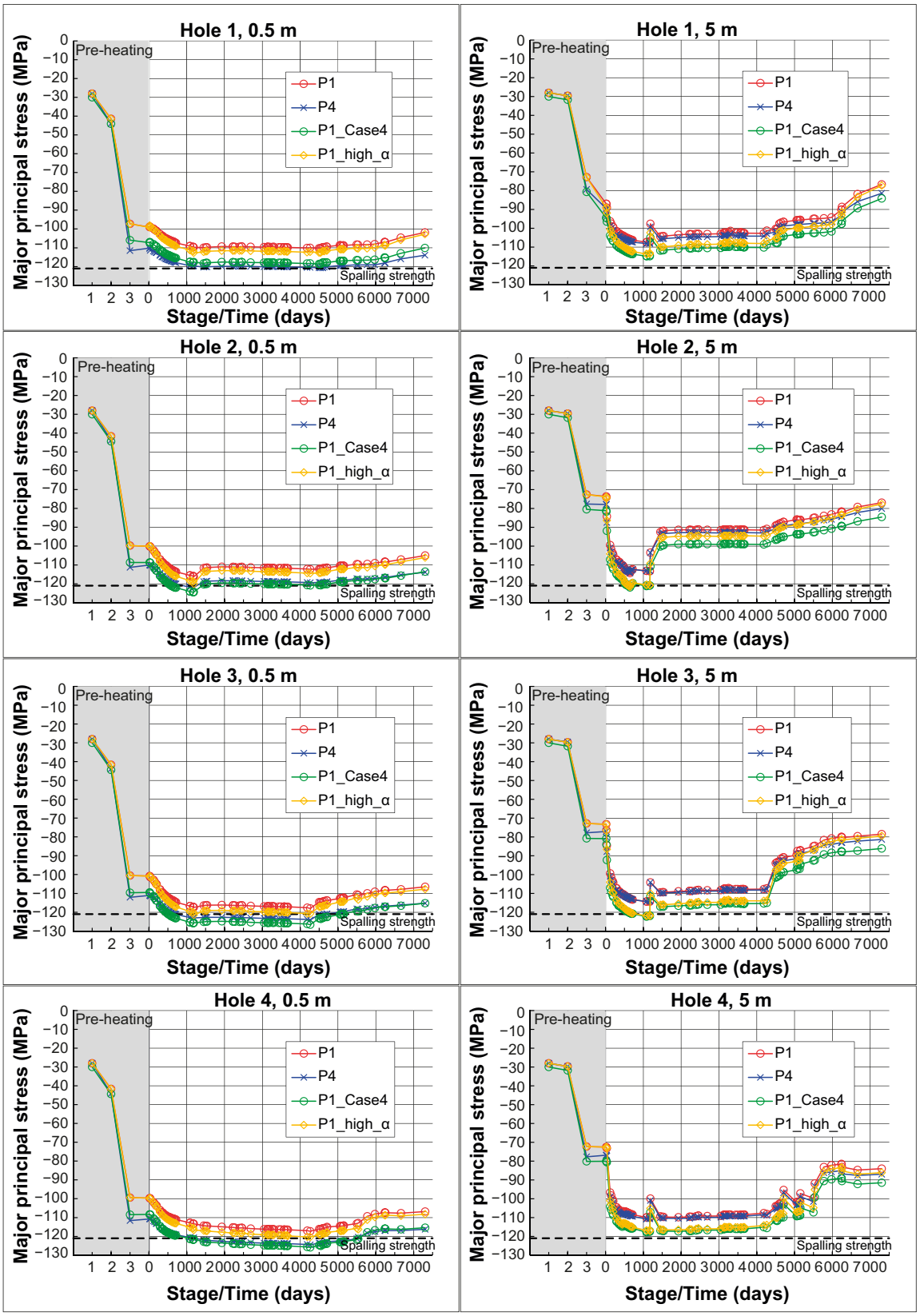

Figure 3-6. *Simulated evolution of the major principal stress in the deposition hole walls in all elastic continuum models. Results are given at two depths below tunnel floor, see Figure 3-5. The grey area represents the pre-heating stages: (1) initial equilibrium, (2) excavation of tunnel and (3) excavation of deposition holes.*

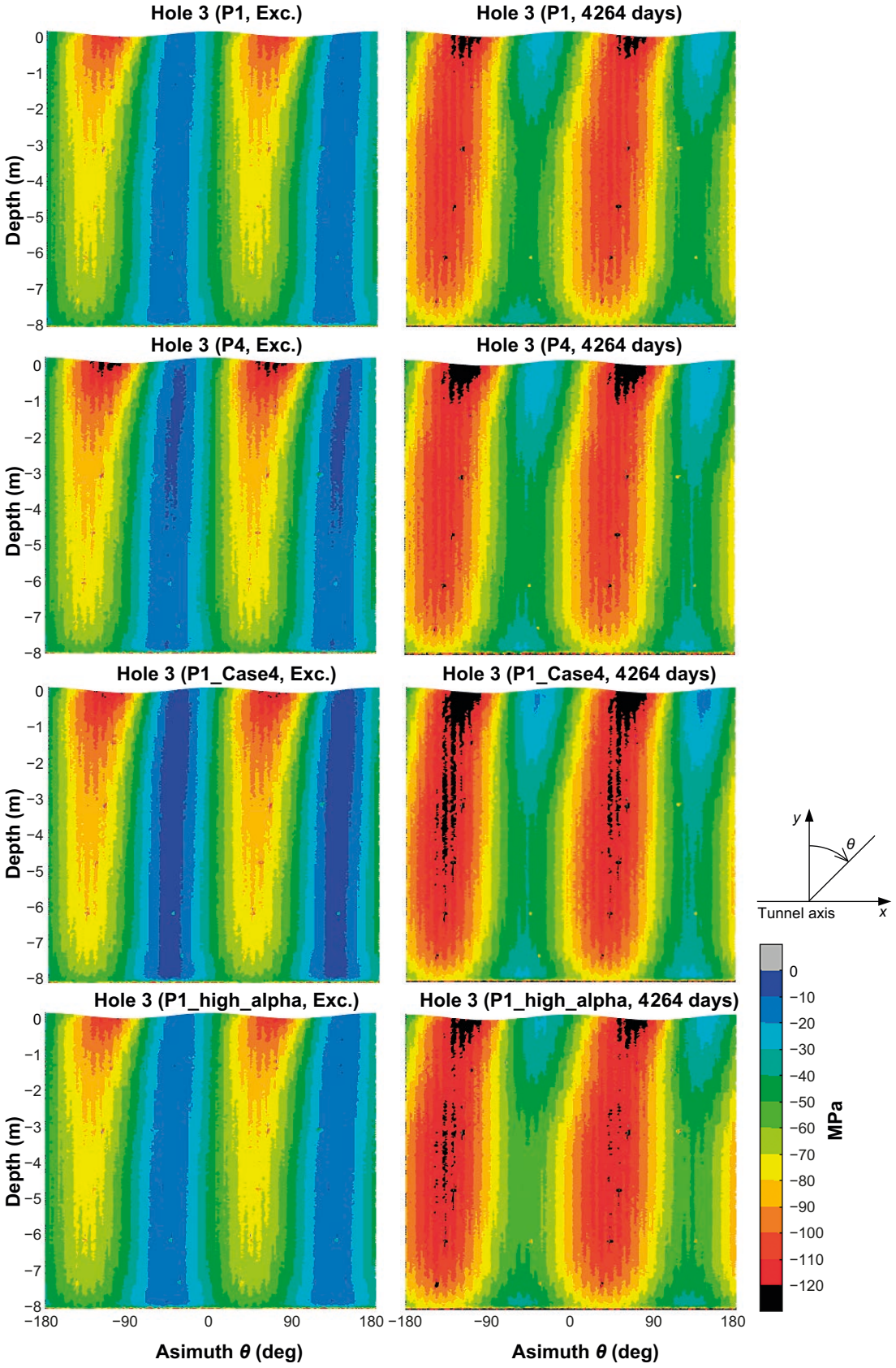

Figure 3-7. *Contours of major principal stress in the wall of deposition hole 3 in all elastic continuum models after excavation and after 4 264 days of heating. Corresponding plots for all models and deposition holes are presented in Appendix A.*

3.3 Effects of fractures

Here, results from the models containing fracture joint planes are presented. The presentation is made in two subsections. In the first subsection, examples of joint shear displacements are shown while stresses in the deposition hole walls are presented in the second subsection.

3.3.1 Fracture shear displacements

Two examples of joint displacements are shown in Figure 3-8 and Figure 3-9. The contour plots show shear displacements after 4 264 days of heating in the P1_fr_pp and P1_fr models. The black dots indicate monitoring points for the displacement evolutions shown in the lower right insets. Corresponding plots for all joint planes are presented in Appendix B. The following can be observed:

- The impact of excavation on the shear displacements is considerably stronger than the impact of the heating. The change in displacements generated by the heating is marginal compared to the displacements generated during the preceding excavation.
- Significant shear displacements were localised to regions close to the openings where the stress alterations caused by the excavation and by the heating were strongest. The displacements became particularly large at locations near the openings where the joints lose compression during the excavation. This can be seen in the lower part of deposition hole 2 where Joint 3046 and Joint 2069 form a wedge close to the hole wall (Figure 3-8). Similarly, there is a region on Joint 4019 close to the tunnel wall between hole 3 and 4 where the compression became low, and displacements tended to be large (Figure 3-9). The reduction of compression on Joint 4019 became more pronounced due to the gently dipping Joint 4001 which is located some 0.5 m below the tunnel floor.
- The impact of the pore pressure assumption made here was considerable. In the P1_fr_pp model, where the pore pressure was assumed to be hydrostatic and uniform during all simulation steps, shear displacements could be tens of mm at locations close to the openings. In the P1_fr model, with zero pore pressure during excavation and heating, no shear displacement exceeded 1.5 mm at the stage after 4 264 days of heating.

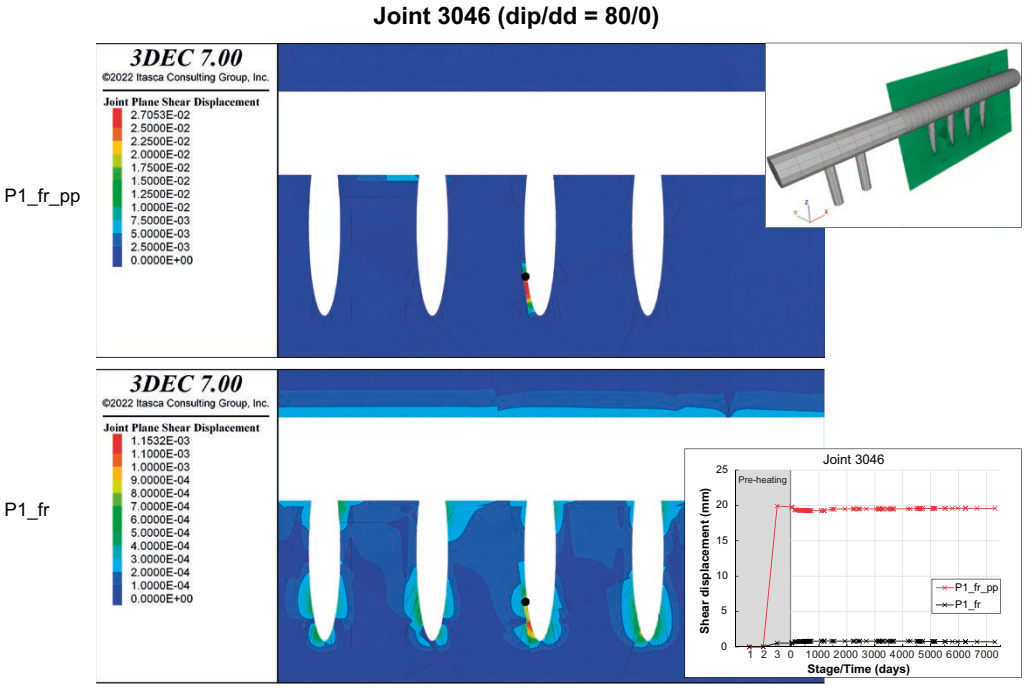

Figure 3-8. *Contours of shear displacements (m) on Joint 3046 after 4 264 days of heating in the P1_fr_pp (upper) and P1_fr (lower) models. The upper right inset shows the joint location/orientation relative to the tunnel. The black dot indicates the recording point for the displacements in the lower right inset.*

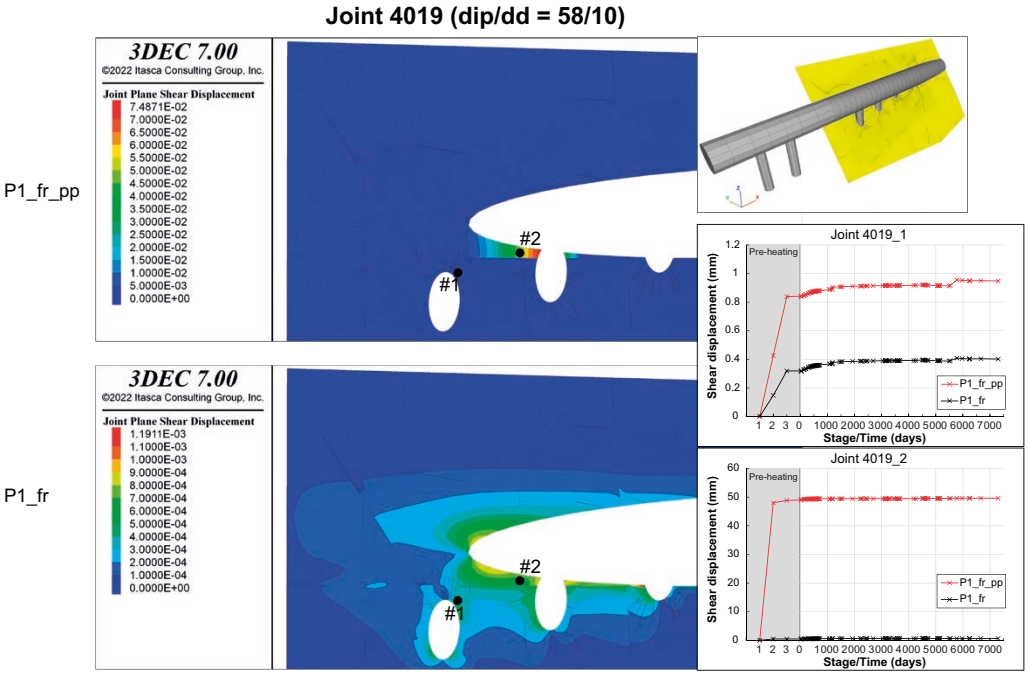

Figure 3-9. *Contours of shear displacements (m) on Joint 4019 after 4 264 days of heating in the P1_fr_pp (upper) and P1_fr (lower) models. The upper right inset shows the joint location/orientation relative to the tunnel. The black dots indicate the recording points for the displacements in the lower right insets.*

3.3.2 Stresses in deposition hole walls

The shear displacements generated on the joint planes alter the stresses around the deposition holes. The impact on the stresses in the deposition hole walls is illustrated by the results presented in this section. Results from the two models with the fractures active (P1_fr, P1_fr_pp) are presented along with results from the P1_fr_glued model in which the joint planes were made mechanically inactive.

Figure 3-10 and Figure 3-11 show contours of major principal stress in the walls of deposition hole 2 and 4, respectively (Corresponding plots for all models and deposition holes are presented in Appendix A). Two stages are considered: excavation of deposition holes and 4 264 days of heating. The grey lines indicate the traces of the intersections between the joint planes and the deposition hole walls. The plots illustrate that fracture movements can have an impact on the stresses. The stresses were either increased or relaxed in places along the fracture intersections. Stresses were increased particularly around the tips of the intersections between the deposition hole walls and steep fractures. At these locations, the simulated stresses could exceed the spalling strength already after excavation. During heating the stress increase was considerable in places, with calculated stresses far beyond the uniaxial compressive strength, which here was assumed to be about 210 MPa. The figures also show the potential of pore pressures to alter the stresses. The assumption of full hydrostatic pore pressure uniformly in all joint planes (P1_fr_pp model) had a particularly strong impact in deposition hole 2 where Joint 3046 and Joint 2069 form a wedge at the deposition hole wall (Figure 3-10, bottom, cf Section 3.3.1).

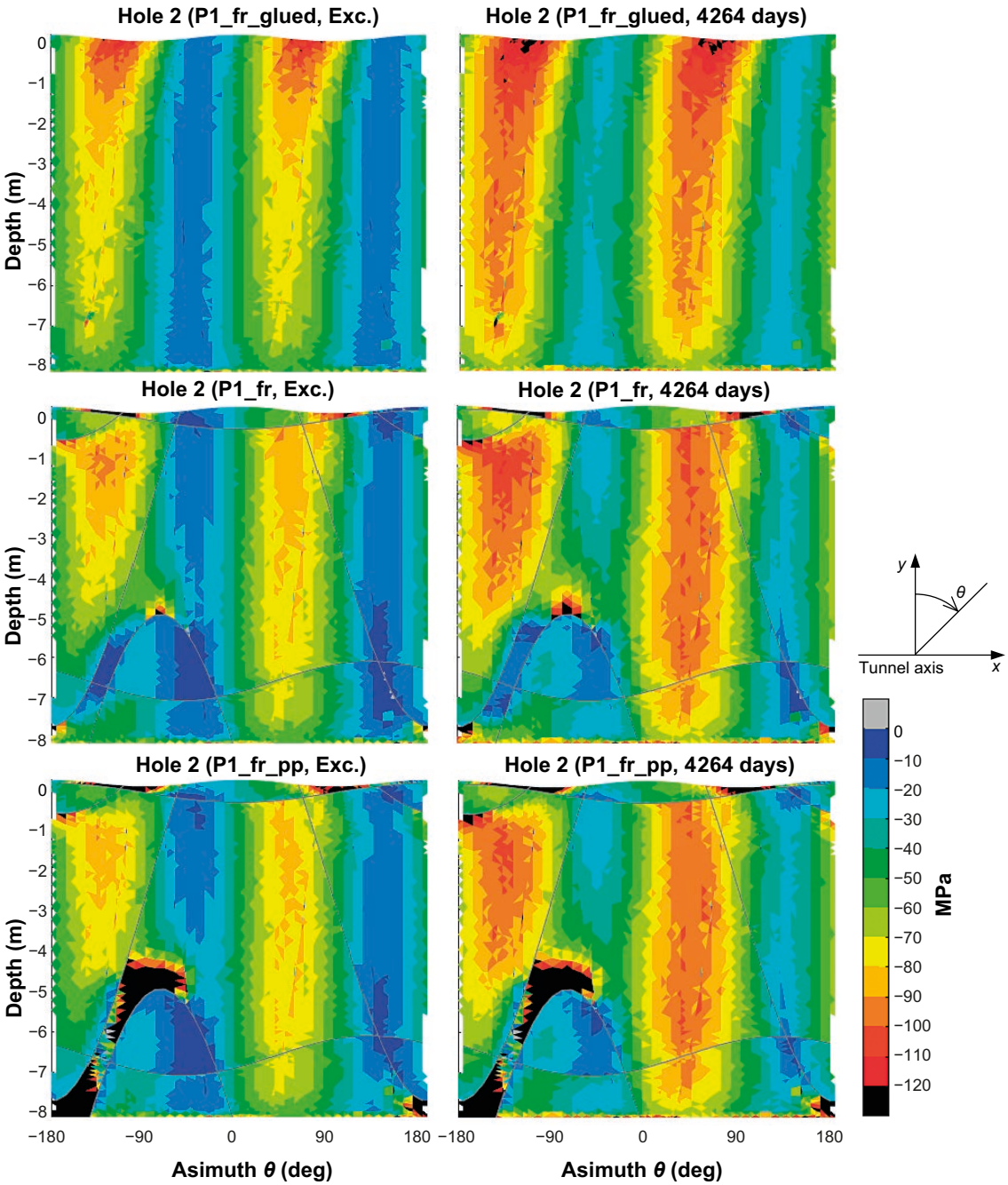

Figure 3-10. *Contours of major principal stress in the wall of deposition hole 2 in the models with fractures after excavation and after 4 264 days of heating. The grey lines indicate the traces of the intersections between the joint planes and the deposition hole walls. Corresponding plots for all models and deposition holes are presented in Appendix A.*

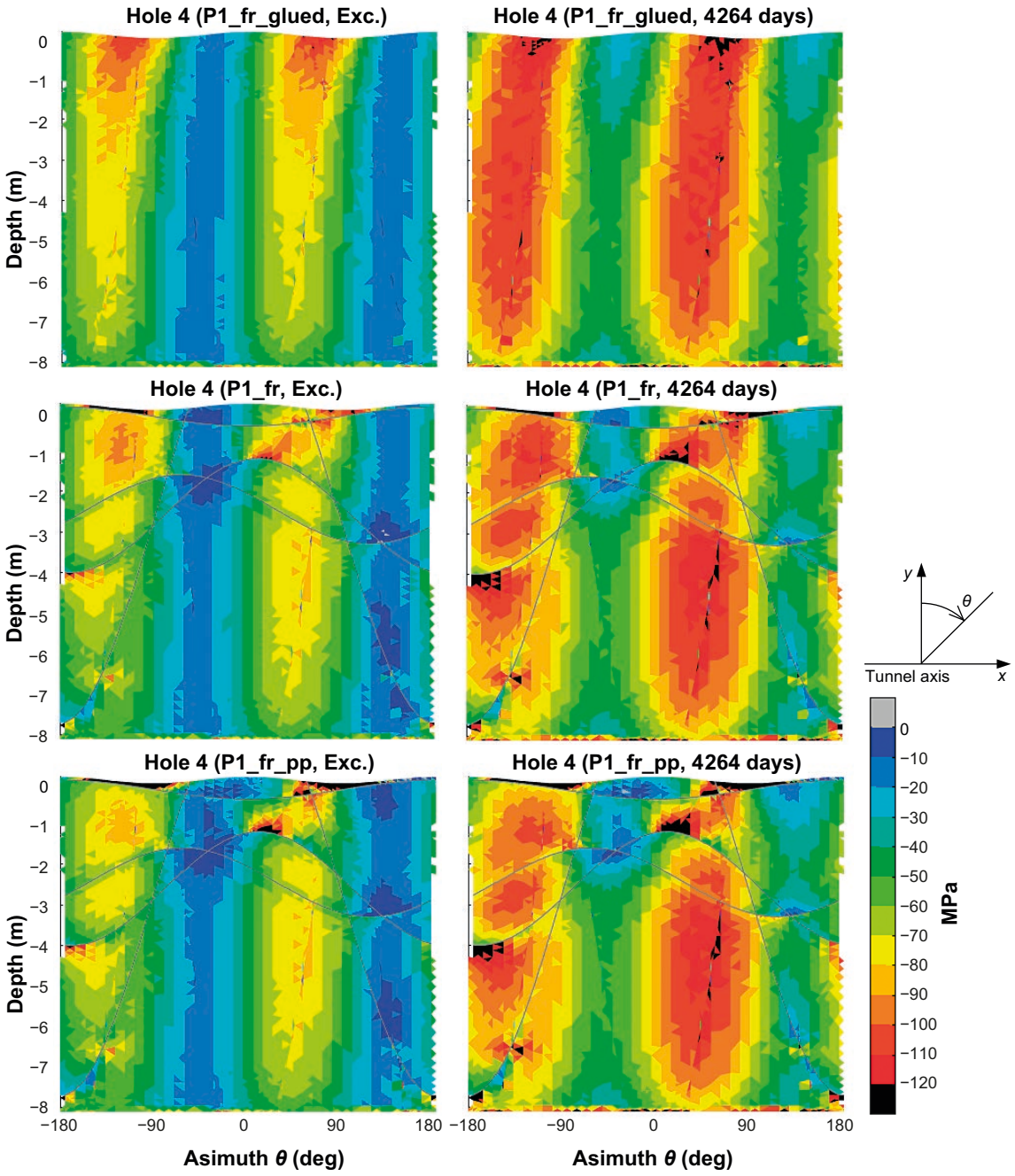

Figure 3-11. *Contours of major principal stress in the wall of deposition hole 4 in the models with fractures after excavation and after 4 264 days of heating. The grey lines indicate the traces of the intersections between the joint planes and the deposition hole walls. Corresponding plots for all models and deposition holes are presented in Appendix A.*

4 Discussion

For the temperature calculations performed here, the analytic logic in 3DEC was used in combination with the application of compound line heat sources. Hence, the temperature evolution was simulated assuming homogeneous thermal properties in the model volume. Even though the thermal properties of the tunnel backfill, the bentonite buffer and the heaters deviate from those of the rock mass, the results show that, using this modelling approach, it is possible to simulate the thermal evolution in the rock mass in the vicinity of the canisters in a KBS-3 repository with an acceptable accuracy. This is in accord with the findings by Lönnqvist and Hökmark (2015). However, this is given that there are no large water movements and associated heat convection in the vicinity of the canisters or in the tunnel. As concluded by Lönnqvist and Hökmark (2015), it appears that water movements in the inner section redirect the heat flow such that the temperatures are overpredicted by the model, particularly around the innermost part of the tunnel. To obtain a better agreement between simulation results and measurements, a less schematic modelling approach, involving non-homogeneous properties and possibly more detailed data on water movements, would be needed. However, as argued in Section 1.3, the modelling approach applied here was considered to be relevant for the purpose of this study.

The overprediction of the temperature increase made by the model amounts to 2–3 °C, at most, at some locations close to the deposition holes in the inner section. This corresponds to some 20 % overprediction of the temperature increase. The overprediction appears to be most prominent around deposition holes 1 and 2. Around holes 3 and 4, the agreement between calculated and measured temperatures is fairly good. The overprediction means that the stresses around the deposition holes, which was of main interest here, should be overpredicted rather than underpredicted by the models. Since linear thermal expansion in the rock mass was considered a valid assumption and was applied here, the overprediction of the thermal stresses should scale approximately with the overprediction of the temperature increase.

The deposition holes were assumed to be unfilled after excavation, i.e., no account was taken for the possible impact of swelling pressures in the bentonite buffer. According to analytical solutions, an increase of the total pressure inside a cylindrical cavity gives a reduction of the tangential compressive stress in the volume close to the cavity wall that is nearly equal to the pressure increase (e.g. Lönnqvist and Hökmark 2015). The total pressure measurements in the buffer in hole 1 and 3 (no measurements were made in hole 2 and 4) show a large spread with values in the range 0–8 MPa depending on position (Goudarzi 2012). Hence, based on this data, it is difficult to make any robust quantification of how the approach used here may have contributed to any overprediction of the deposition hole wall stresses.

In the elastic continuum base case P1 model, the highest tangential stresses were found in deposition hole 3 after some 4 200 days of heating. In the P1 model, “intact rock” Young’s modulus was applied homogeneously. According to Figure 7-9 in Lönnqvist and Hökmark (2015), this would give some 3 MPa higher stresses in the most highly stressed parts of the deposition hole walls close to the tunnel floor and some 10 MPa higher stresses at canister mid-height, compared to a case with “rock mass” Young’ modulus everywhere. Hence, from a spalling assessment point of view, the model assumption made here should contribute to a pessimistic assessment.

The P4 model, where the Young’s modulus in the continuum was set to the “rock mass” value everywhere except for in a small volume surrounding the deposition holes, represents a case similar to the P4 case considered by Lönnqvist and Hökmark (2015). Out of the stiffness variations tested in the simulations by Lönnqvist and Hökmark (2015) this was the case that gave the highest deposition hole wall stresses. The stiffness variation in the P4 model is a schematic way of examining the effects of having inclusions of stiffer rock around the deposition holes. It is pointed out here that it does not represent any property variation that has been documented in the Prototype repository rock mass.

The orientations and positions of the joint planes simulating fractures were schematically based on fracture mappings presented in Rhén and Forsmark (2001). However, it is not claimed here that the network of joint planes included in the models represented any real network in the Prototype rock mass. The intention was not to include all fractures that were included in the mapping, but rather to have a number of joints with a range of orientations and positions. In addition, all joints were schematically assumed to extend through a large volume surrounding the inner section. Hence, a joint based on the mapping of, e.g., hole 3 could extend through all holes in the inner section. The joint network should be considered generic.

According to the model results, fractures that intersect the deposition holes can perturb the stresses in the deposition hole walls considerably. Particularly around the tips of the intersections between the deposition hole walls and steep fractures, the simulated stresses could exceed the spalling strength already after excavation. However, based on comparisons between modelling results and observations made in deposition hole 5 and 6 after dismantling of the outer section, Lönnqvist and Hökmark (2015) argued that the model assumption of perfectly planar joints may lead to an overestimation of the impact of fractures.

The schematic assumption of hydrostatic pore pressure on all parts of the joints led to a considerable increase of the joint shear movements and to a much stronger impact on the stresses as compared to the zero-pore pressure case. However, given that the shear displacements, for both pore pressure assumptions tested here, were localised to regions close to the openings where the pore pressure in most cases is considerably lower than the hydrostatic level (e.g. Goudarzi 2012), it is judged here that the zero-pore pressure case is the most relevant of the two cases tested here.

5 Conclusions

Based on the results presented here, the following conclusions could be made:

- As found by Lönnqvist and Hökmark (2015) a good agreement between calculated rock mass temperatures and corresponding measurements can be obtained by using 3DEC's analytic logic with the heaters modelled as compound line sources. The model overestimated the temperatures at some positions in the innermost part of the tunnel. The overestimation of the temperature increase reached about 20 % at some locations near deposition holes 1 and 2. The overestimation was attributed to water movements and associated heat convection in the experiment.
- The overestimation of temperatures implies that the thermal stresses around the deposition holes were overestimated, particularly around hole 1 and 2. Around hole 3 and 4, where the highest stresses were found, the agreement between calculated and measured temperatures can be considered acceptable.
- Given elastic continuum conditions (no effects of fractures considered), the highest deposition hole wall tangential stresses were always found near the tunnel floor. Adopting base case assumptions (P1 model with elastic and continuous rock mass and "intact rock" properties), no stress above 110 MPa was found after excavation. The heating increased the tangential stresses such that the spalling strength (121 MPa) was exceeded near the tunnel floor. The highest stresses were generated in hole 3 after some 4 200 days of heating with stresses exceeding the spalling strength down to about 0.5 m below the tunnel floor.
- Variations in rock mass properties and background stress field may lead to higher deposition hole wall stresses. In the model cases with alternative rock mass stiffness distribution, higher background stress anisotropy and higher thermal expansion coefficient the stresses were increased compared to those of the base case by almost 10 MPa in certain locations. The highest stresses were obtained close to the tunnel floor in hole 3 and 4 in the model with alternative rock mass stiffness distribution (P4) and in the model with higher stress anisotropy (P1_Case4). At 0.5 m depth below the tunnel floor in these models, the stress exceeded the spalling limit during the time interval 1 000 – 4 500 days (approximately) of heating. The volumes with stresses exceeding the spalling strength increased, particularly in the case with higher stress anisotropy. In that case the model indicated possible initiation of spalling down to about 5 m depth in hole 3 and 4.
- Shear movements on fractures intersecting a deposition hole may locally perturb the stresses in the hole wall quite considerably. Particularly around the tips of the intersections between the deposition hole walls and steep fractures, the simulated stresses could exceed the spalling strength already after excavation. However, for the zero-pore pressure assumption, which was considered the most relevant here, the shear displacements and the associated stress-perturbed volumes were modest. Hence, it is uncertain if any effects of fracture intersections will be observed after dismantling of the experiment (cf discussion on this issue in Lönnqvist and Hökmark (2015)).

In addition to the overestimation of temperatures, there are other factors suggesting that the stresses simulated here may be overestimates rather than underestimates:

- In all model cases considered here, "intact rock" Young's modulus was assumed for the rock mass around the deposition holes. Assuming the lower "rock mass" value everywhere instead of the "intact rock" value would give lower thermal stresses. In the simulations by Lönnqvist and Hökmark (2015), making this assumption, they obtained about 3 MPa reduction in the most highly stressed region close to the tunnel and some 10 MPa reduction at canister mid-height. In addition, the way the rock mass stiffness distribution was modelled here, with higher stiffness around the deposition holes, tends to give increased excavation stresses (Figure 7-9 in Lönnqvist and Hökmark 2015).
- No account was taken for the possible reductions of tangential stresses caused by swelling pressure in the bentonite buffer.

Given the modelling results presented here, with some model cases generating stresses several mega-pascals above the spalling strength, the possibility that spalling may have been initiated during heating cannot be excluded. This would be the case particularly in hole 3 and 4, in which the highest stresses were simulated and where the agreement between calculated and measured temperatures was best. It should, however, be noted that the small support of the pellet filling along the hole wall may be sufficient to suppress the initiation of spalling (Glamheden et al. 2010).

References

SKB's (Svensk Kärnbränslehantering AB) publications can be found at www.skb.com/publications.

CIMNE, 2004. Code_Bright. Version 2.2 users guide. Departemento de Ingenieria del Terreno, Cartográfica y Geofísica. Universidad Politécnica de Cataluña, Spain.

Fransson Å, Thörn J, Ericsson L O, Lönnqvist M, Stigsson M, 2012. Hydromechanical characterization of fractures close to a tunnel opening: a case study. In Proceedings of Eurock 2012, ISRM International Symposium, Stockholm, 28–30 May 2012.

Glamheden R, Fälth B, Jacobsson L, Harrström J, Berglund J, Bergkvist L, 2010. Counterforce applied to prevent spalling. SKB TR-10-37, Svensk Kärnbränslehantering AB.

Goudarzi R, 2012. Prototype Repository – Sensor data report (period 100917–110101). Report no 24. SKB P-12-12, Svensk Kärnbränslehantering AB.

Goudarzi R, 2021. Prototype Repository – Sensor data report. Period 2001-09-17 to 2020-01-01. Report no 31. SKB P-20-33, Svensk Kärnbränslehantering AB.

Hökmark H, Fälth B, 2003. Thermal dimensioning of the deep repository. Influence of canister spacing, canister power, rock thermal properties and nearfield design on the maximum canister surface temperature. SKB TR-03-09, Svensk Kärnbränslehantering AB.

Hökmark H, Fälth B, Wallroth T, 2006. T-H-M couplings in rock. Overview of results of importance to the SR-Can safety assessment. SKB R-06-88, Svensk Kärnbränslehantering AB.

Hökmark H, Lönnqvist M, Fälth B, 2010. THM-issues in repository rock. Thermal, mechanical, thermo-mechanical and hydro-mechanical evolution of the rock at the Forsmark and Laxemar sites. SKB TR-10-23, Svensk Kärnbränslehantering AB.

Itasca, 2013. 3DEC – 3-Dimensional Distinct Element Code, version 5. User's guide. Minneapolis, MN: Itasca Consulting Group Inc.

Itasca, 2020. 3DEC – 3-Dimensional Distinct Element Code, version 7. User's guide. Minneapolis, MN: Itasca Consulting Group Inc.

Kristensson O, Hökmark H, 2007. Prototype Repository. Thermal 3D modelling of Äspö Prototype Repository. SKB IPR-07-01, Svensk Kärnbränslehantering AB.

Lönnqvist M, Hökmark H, 2015. Thermal and thermo-mechanical evolution of the Äspö Prototype Repository rock mass. Modelling and assessment of sensors data undertaken in connection with the dismantling of the outer section. SKB R-13-10, Svensk Kärnbränslehantering AB.

Pusch R, Börgesson L, Svemar C (eds), 2004. Äspö Hard Rock Laboratory. Prototype Repository. Final report (Deliverable D36). SKB IPR-04-27, Svensk Kärnbränslehantering AB.

Rhén I, Forsmark T, 2001. Äspö Hard Rock Laboratory. Prototype Repository. Hydrogeology. Summary report of investigations before the operation phase. SKB IPR-01-65, Svensk Kärnbränslehantering AB.

Staub I, Andersson J C, Magnor B, 2004. Äspö Pillar Stability Experiment. Geology and mechanical properties of the rock in TASQ. SKB R-04-01, Svensk Kärnbränslehantering AB.

Svemar C, Johannesson L-E, Grahm P, Svensson D, Kristensson O, Lönnqvist M, Nilsson U, 2016. Prototype Repository. Opening and retrieval of outer section of Prototype Repository at Äspö Hard Rock Laboratory. Summary report. SKB TR-13-22, Svensk Kärnbränslehantering AB.

Appendix A

Stresses in the deposition hole walls – all model cases

The figures in this appendix show contours of major principal stress in the deposition hole walls for all models after excavation and after 4 264 days of heating. In Figure A-5, Figure A-6 and Figure A-7, which show results from the models with fractures, the grey lines indicate the traces of the intersections between the joint planes and the deposition hole walls.

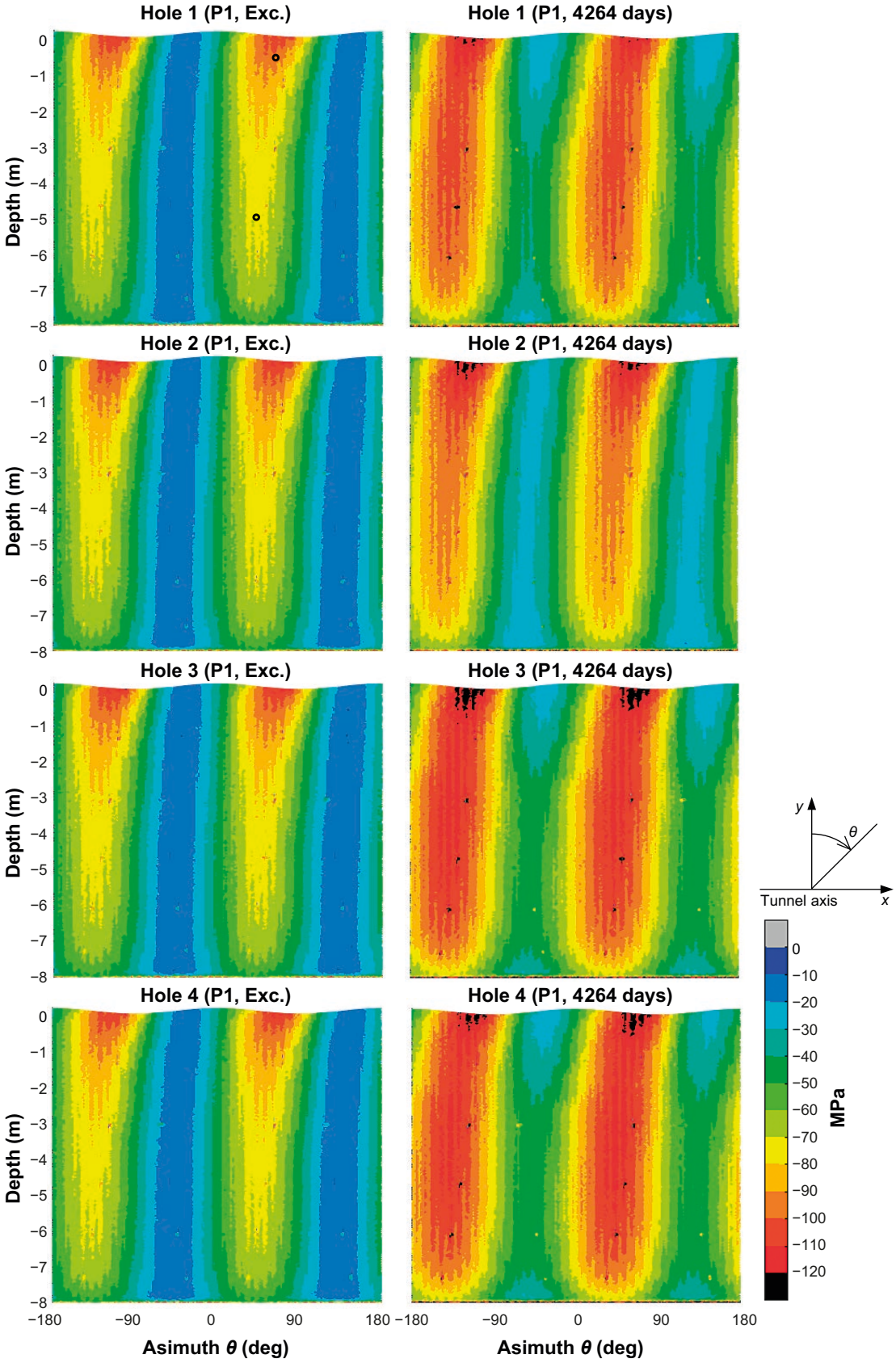

Figure A-1. *Contours of major principal stress in the deposition hole walls in the P1 model after excavation and after 4 264 days of heating.*

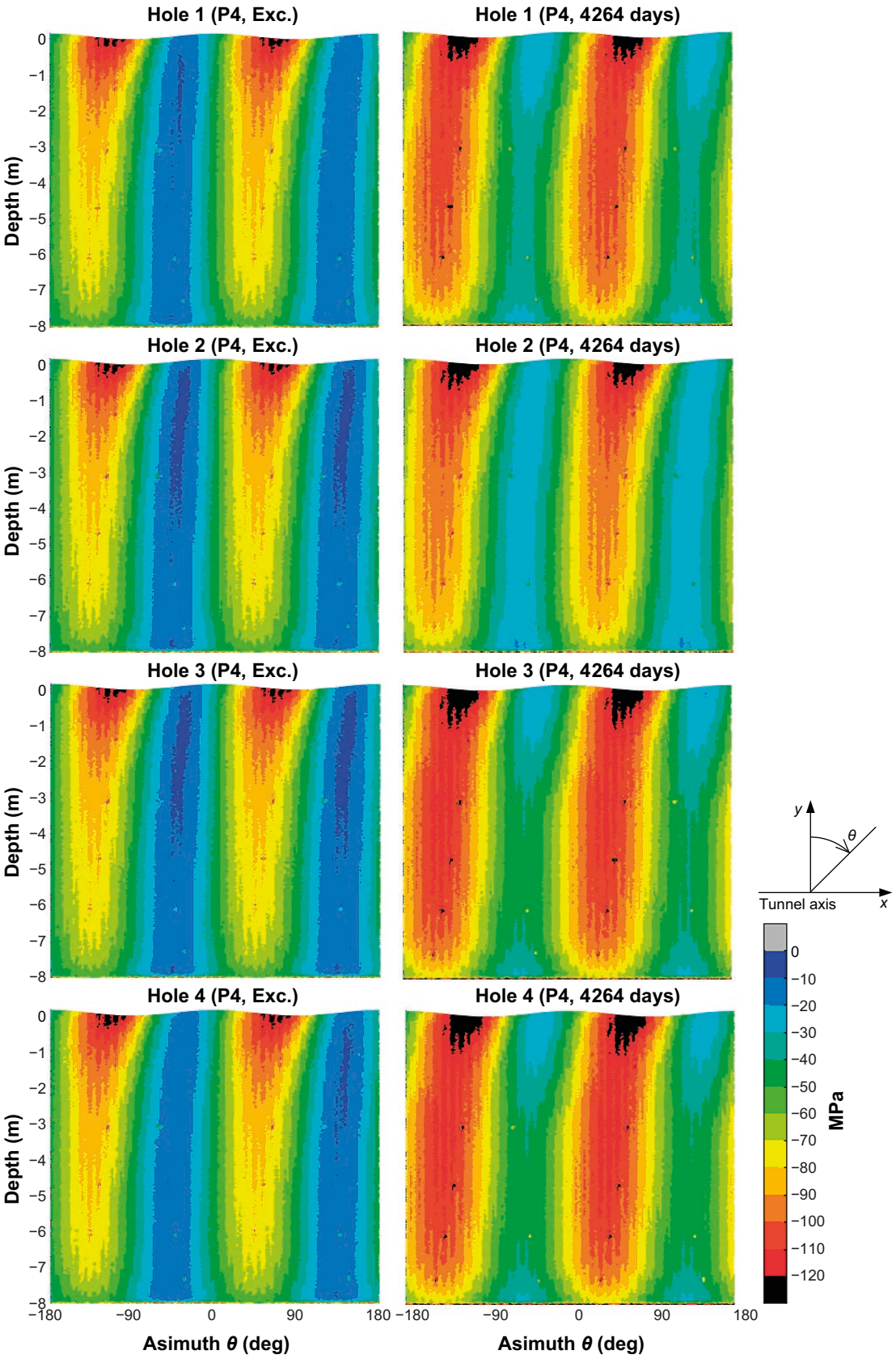

Figure A-2. *Contours of major principal stress in the deposition hole walls in the P4 model after excavation and after 4 264 days of heating.*

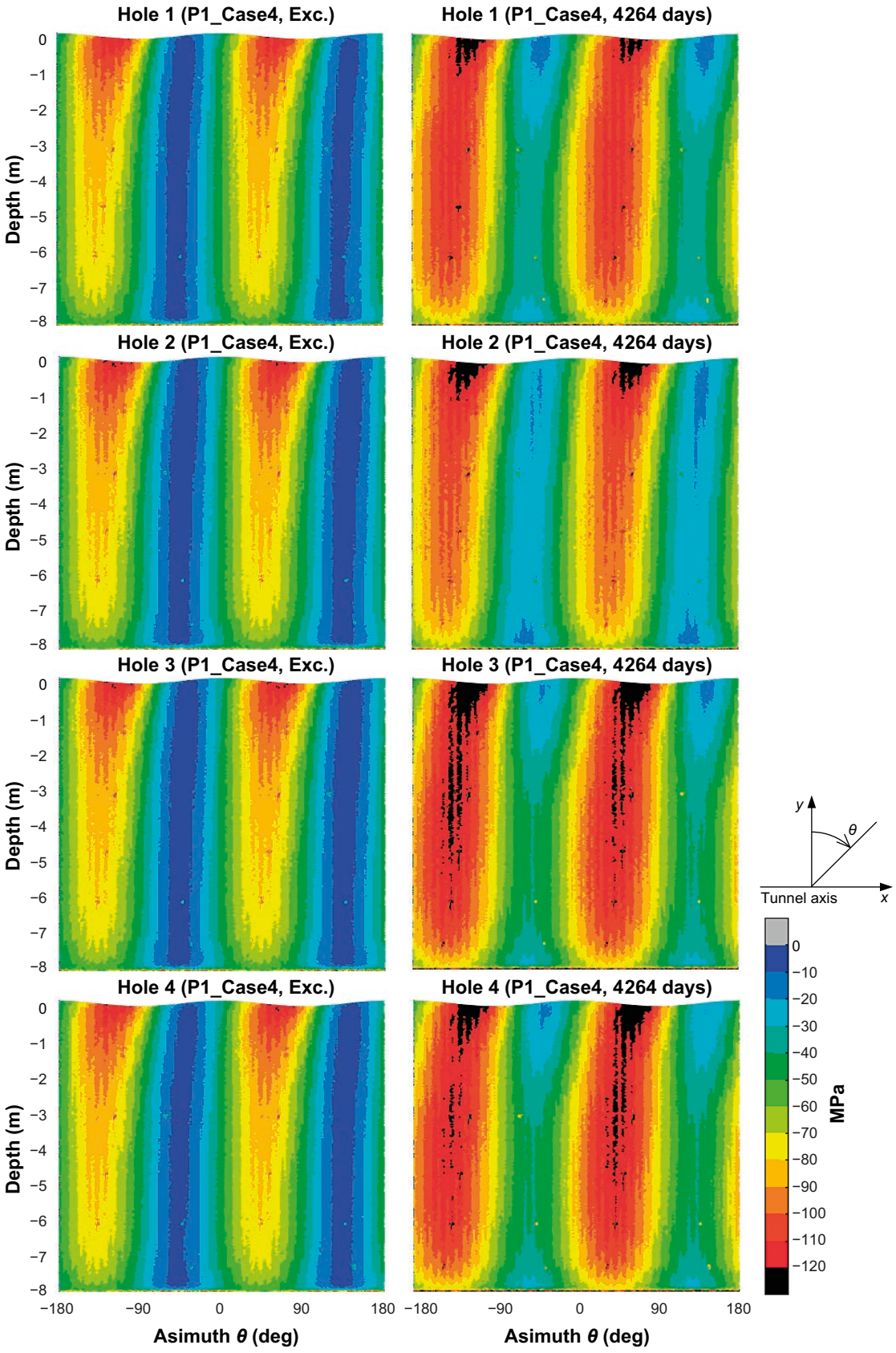

Figure A-3. *Contours of major principal stress in the deposition hole walls in the P1_Case4 model after excavation and after 4264 days of heating.*

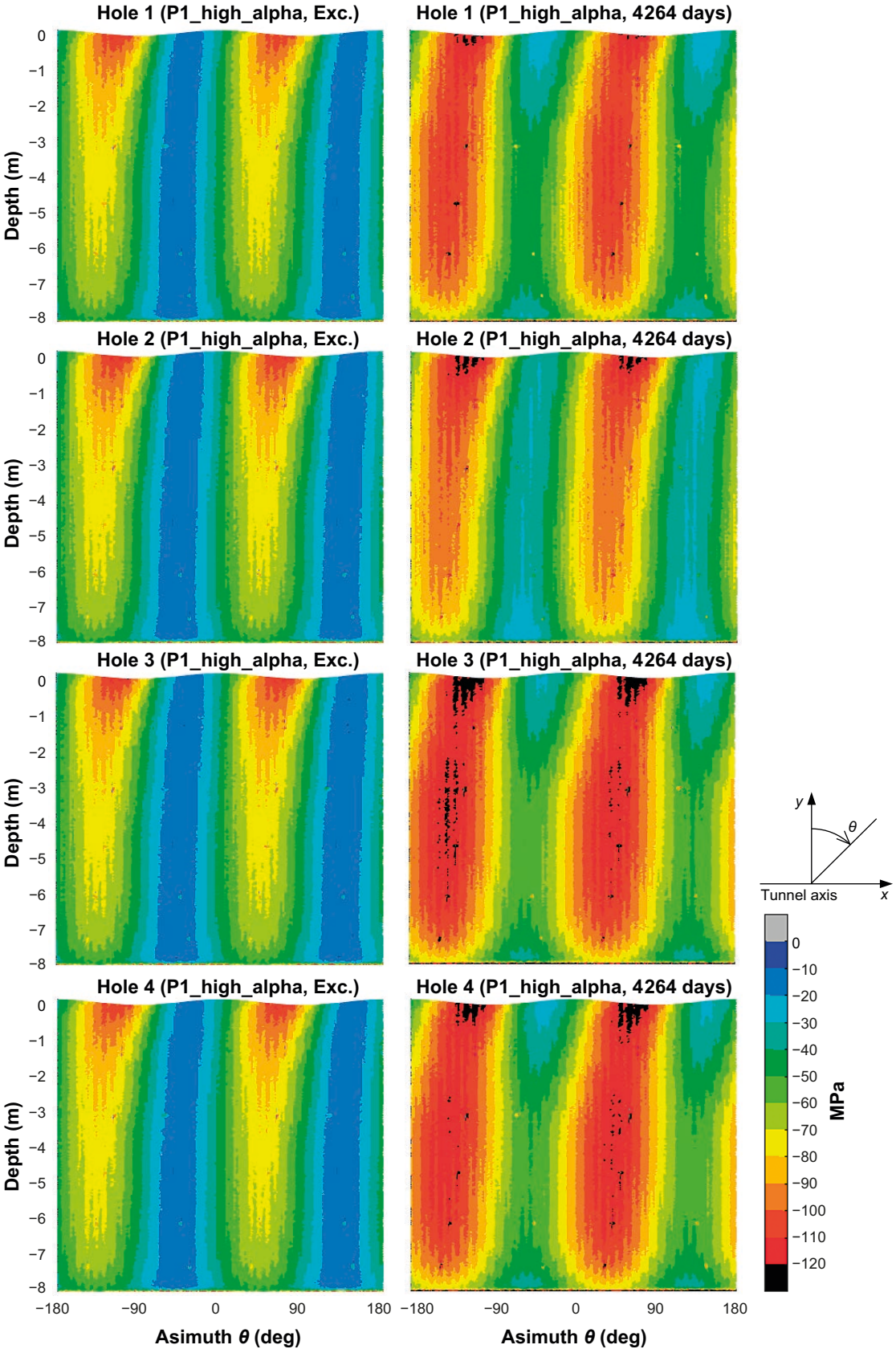

Figure A-4. *Contours of major principal stress in the deposition hole walls in the P1_high_α model after excavation and after 4264 days of heating.*

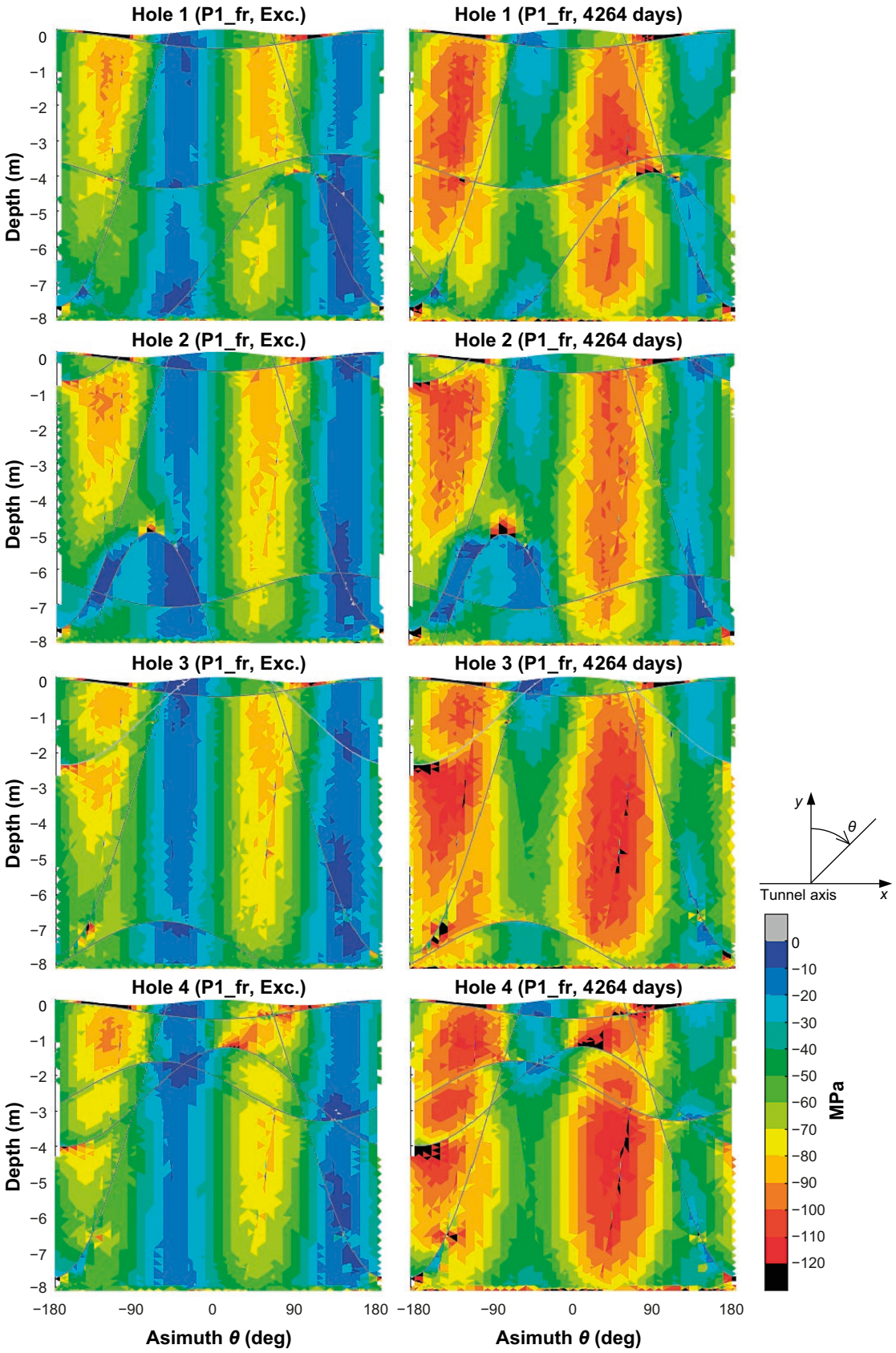

Figure A-5. *Contours of major principal stress in the deposition hole walls in the P1_fr model after excavation and after 4264 days of heating. The grey lines indicate the traces of the intersections between the joint planes and the deposition hole walls.*

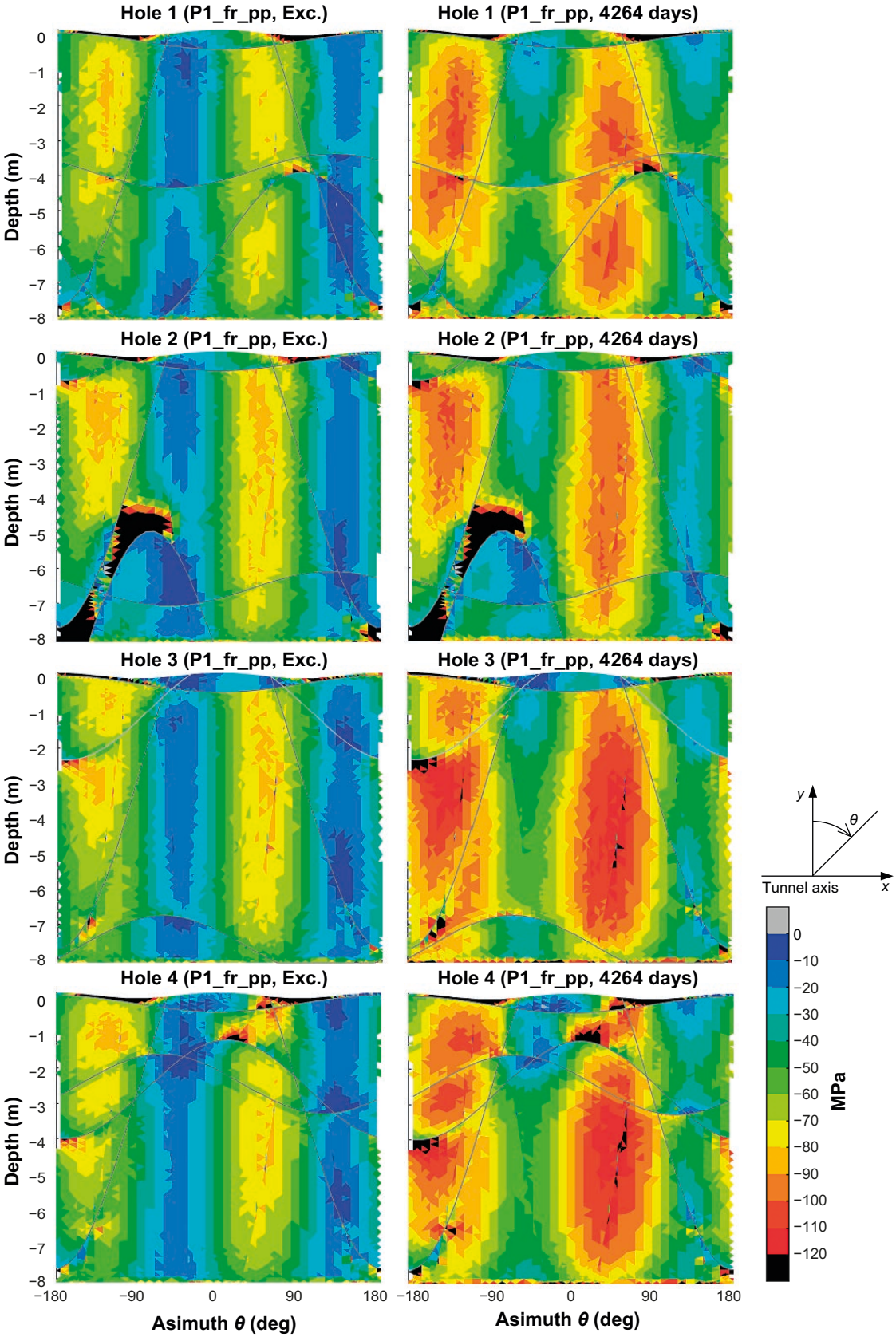

Figure A-6. *Contours of major principal stress in the deposition hole walls in the P1_fr_pp model after excavation and after 4264 days of heating. The grey lines indicate the traces of the intersections between the joint planes and the deposition hole walls.*

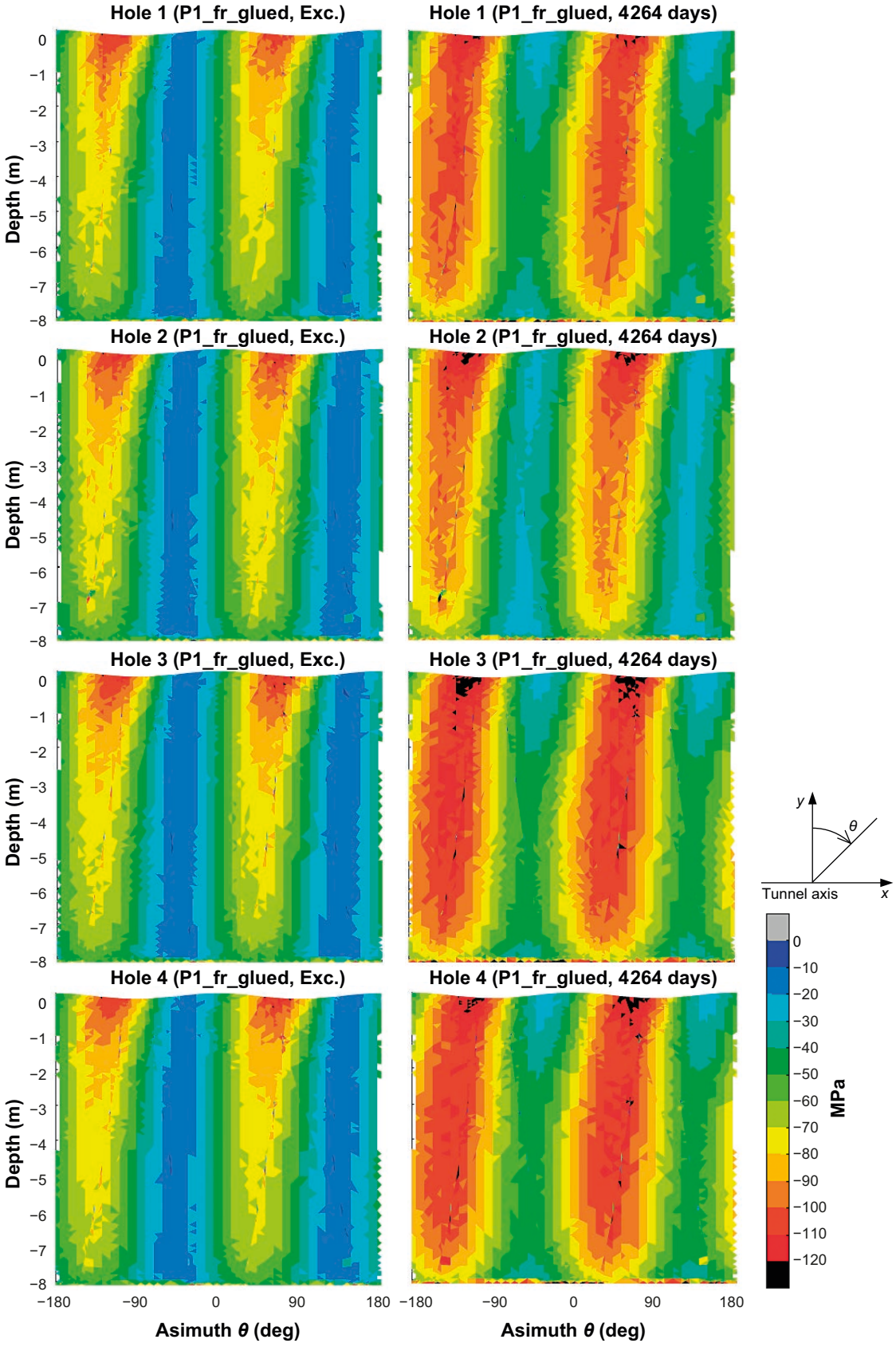

Figure A-7. *Contours of major principal stress in the deposition hole walls in the P1_fr_glued model after excavation and after 4264 days of heating.*

Joint shear displacements

The figures in this appendix show contours of joint shear displacements after 4 264 days of heating as well as temporal evolution of shear displacement at certain locations.

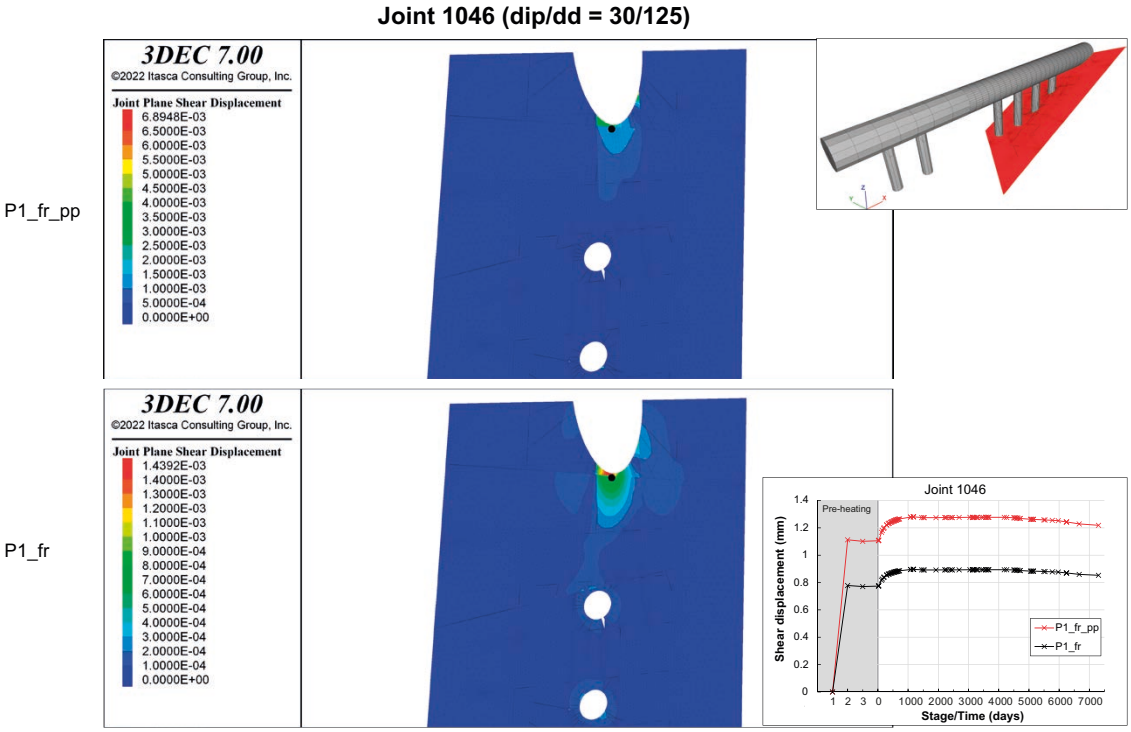

Figure B-1. *Contours of shear displacements (m) on Joint 1046 after 4 264 days of heating in the P1_fr_pp (upper) and P1_fr (lower) models. The upper right inset shows the joint location/orientation relative to the tunnel. The black dot indicates the recording point for the displacements in the lower right inset.*

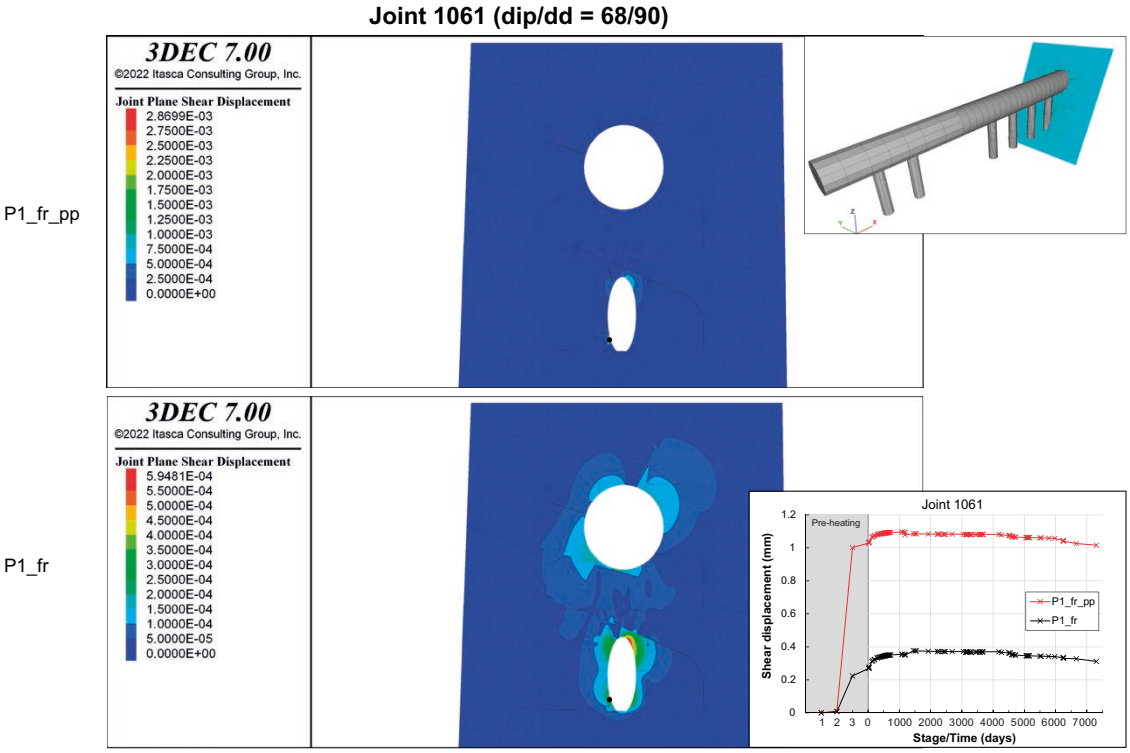

Figure B-2. *Contours of shear displacements (m) on Joint 1061 after 4 264 days of heating in the P1_fr_pp (upper) and P1_fr (lower) models. The upper right inset shows the joint location/orientation relative to the tunnel. The black dot indicates the recording point for the displacements in the lower right inset.*

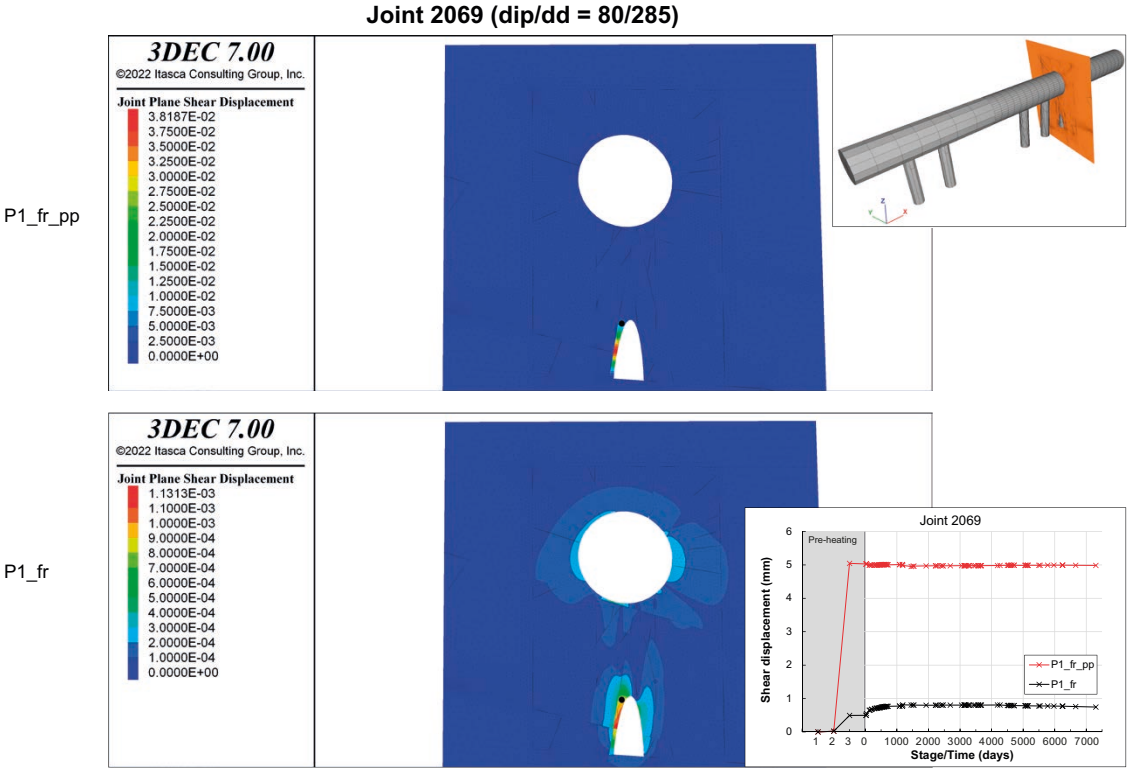

Figure B-3. *Contours of shear displacements (m) on Joint 2069 after 4 264 days of heating in the P1_fr_pp (upper) and P1_fr (lower) models. The upper right inset shows the joint location/orientation relative to the tunnel. The black dot indicates the recording point for the displacements in the lower right inset.*

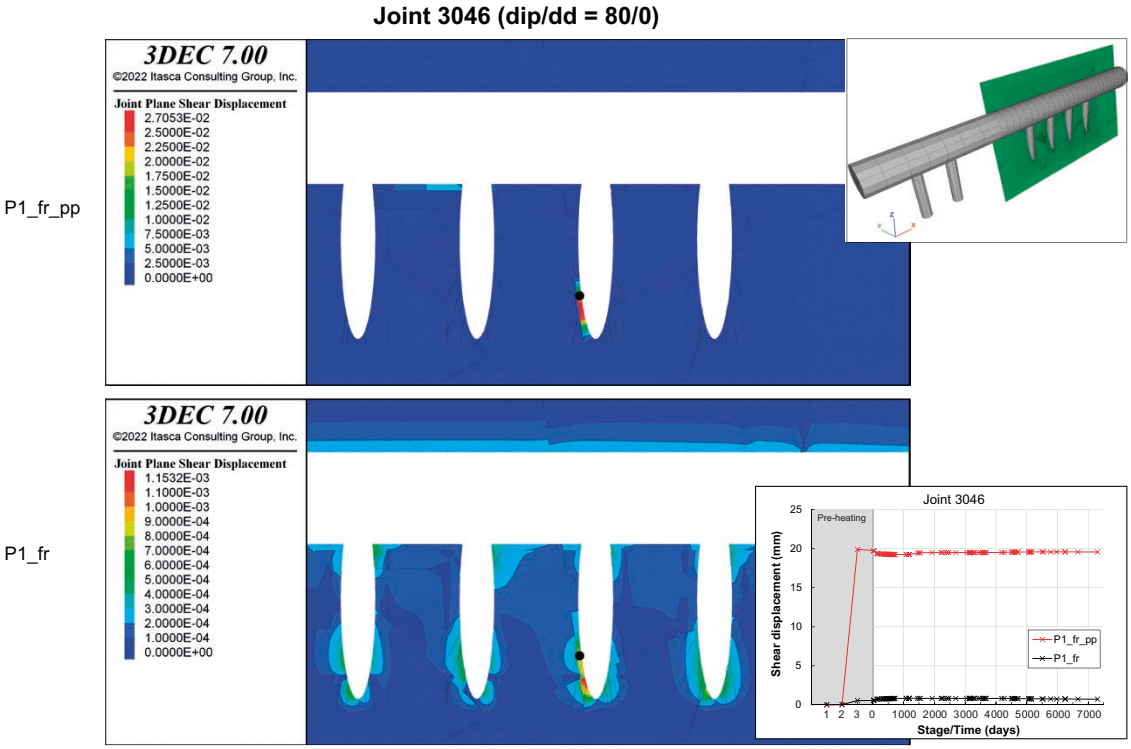

Figure B-4. *Contours of shear displacements (m) on Joint 3046 after 4 264 days of heating in the P1_fr_pp (upper) and P1_fr (lower) models. The upper right inset shows the joint location/orientation relative to the tunnel. The black dot indicates the recording point for the displacements in the lower right inset.*

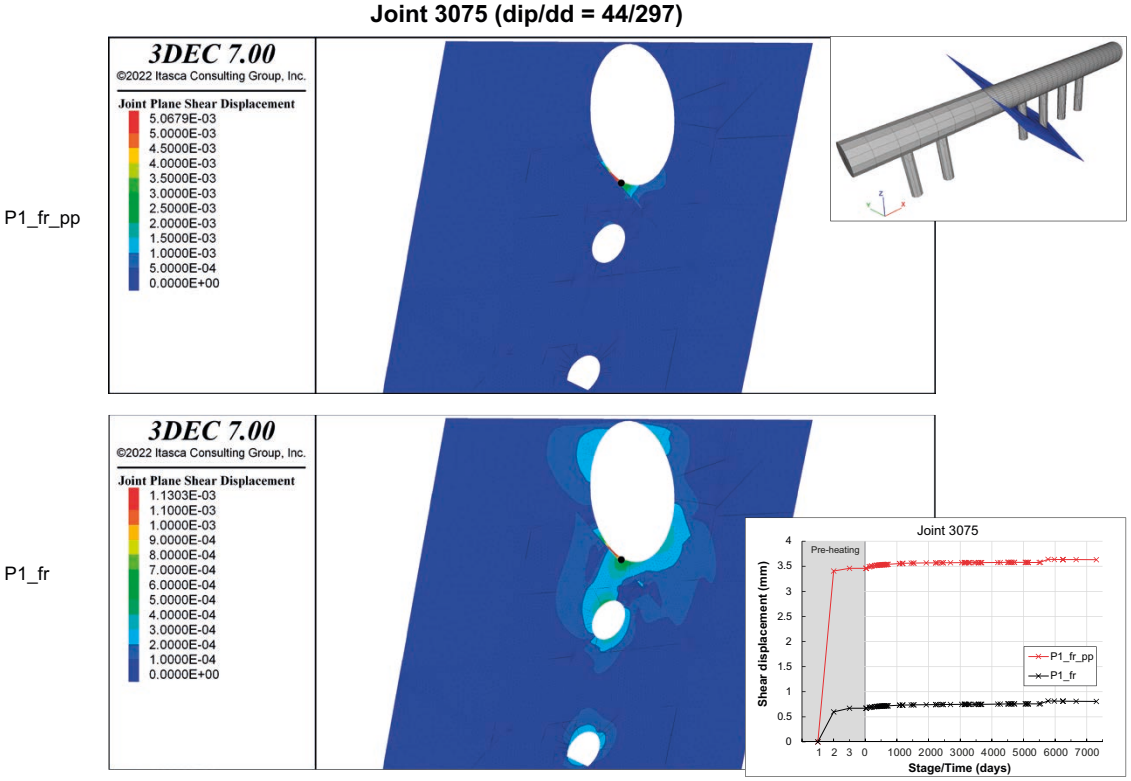

Figure B-5. *Contours of shear displacements (m) on Joint 3075 after 4 264 days of heating in the P1_fr_pp (upper) and P1_fr (lower) models. The upper right inset shows the joint location/orientation relative to the tunnel. The black dot indicates the recording point for the displacements in the lower right inset.*

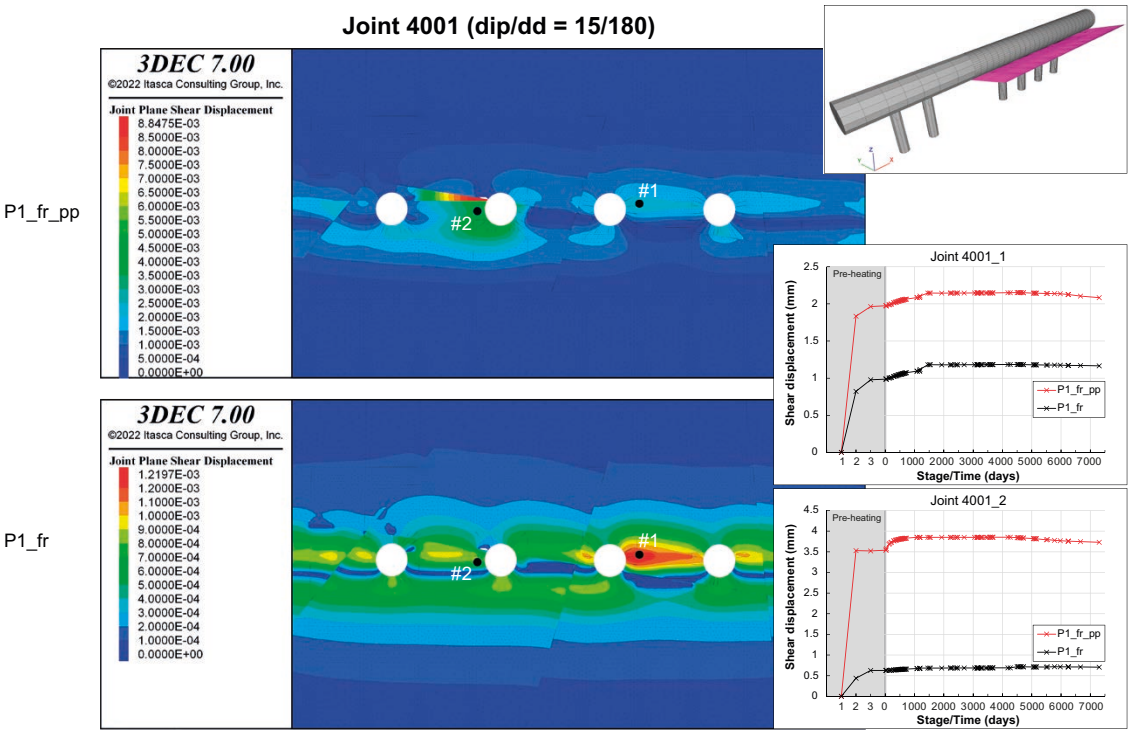

Figure B-6. *Contours of shear displacements (m) on Joint 4001 after 4 264 days of heating in the P1_fr_pp (upper) and P1_fr (lower) models. The upper right inset shows the joint location/orientation relative to the tunnel. The black dots indicate the recording points for the displacements in the lower right insets.*

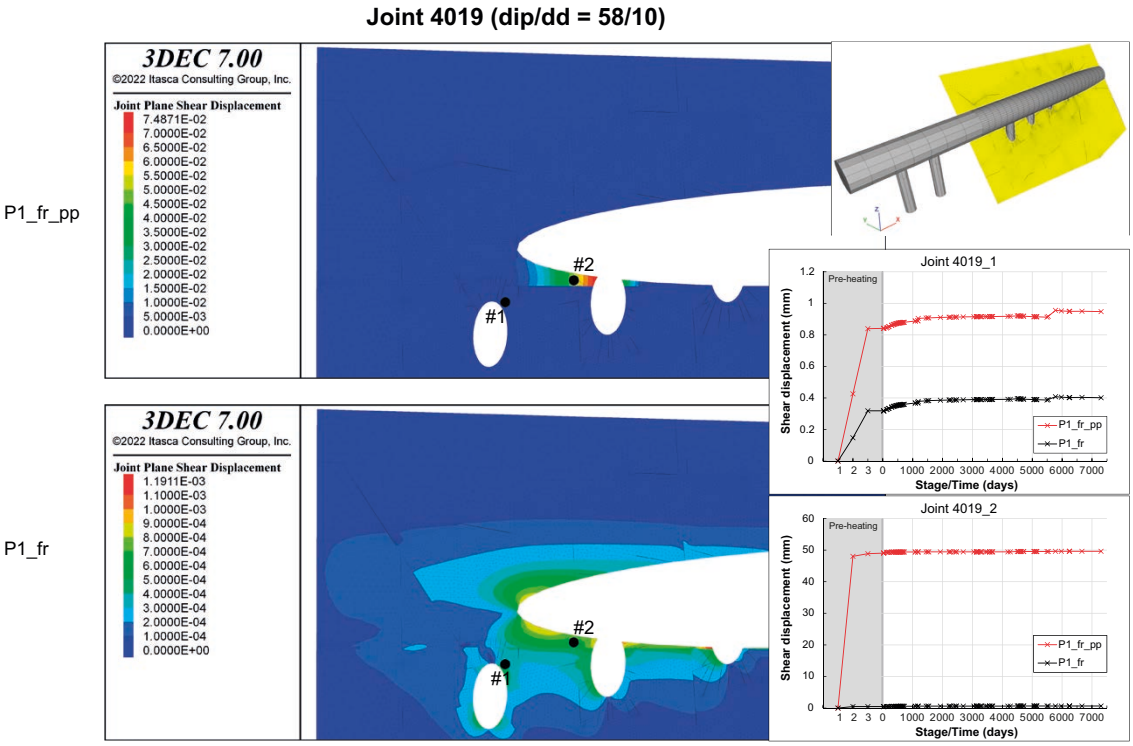

Figure B-7. *Contours of shear displacements (m) on Joint 4019 after 4 264 days of heating in the P1_fr_pp (upper) and P1_fr (lower) models. The upper right inset shows the joint location/orientation relative to the tunnel. The black dots indicate the recording points for the displacements in the lower right insets.*

Arkitektkopia AB, Bromma, 2022

SKB is responsible for managing spent nuclear fuel and radioactive waste produced by the Swedish nuclear power plants such that man and the environment are protected in the near and distant future.

skb.se